IEEE Access
Multidisciplinary | Rapid Review | Open Access Journal

Received June 20, 2016, accepted July 3, 2016, date of publication July 18, 2016, date of current version November 18, 2016.

Digital Object Identifier 10.1109/ACCESS.2016.2591904

Quantum-Aided Multi-User Transmission in Non-Orthogonal Multiple Access Systems

PANAGIOTIS BOTSINIS, (Member, IEEE), DIMITRIOS ALANIS, (Student Member, IEEE), ZUNAIRA BABAR, HUNG VIET NGUYEN, (Member, IEEE), DARYUS CHANDRA, (Student Member, IEEE), SOON XIN NG, (Senior Member, IEEE), AND LAJOS HANZO, (Fellow, IEEE)

School of Electronics and Computer Science, University of Southampton, Southampton SO17 1BJ, U.K.

Corresponding author: L. Hanzo (lh@ecs.soton.ac.uk)

This work was supported in part by the Engineering and Physical Sciences Research Council under Project EP/Noo4558/1 and Project EP/L018659/1, in part by the European Research Council's Advanced Fellow Grant through the Beam-Me-Up Project, and in part by the Royal Society's Wolfson Research Merit Award. All data supporting this study are openly available from the University of Southampton repository at http://dx.doi.org/10.5258/SOTON/399147.

ABSTRACT With the research on implementing a universal quantum computer being under the technological spotlight, new possibilities appear for their employment in wireless communications systems for reducing their complexity and improving their performance. In this treatise, we consider the downlink of a rank-deficient, multi-user system and we propose the discrete-valued and continuous-valued quantum-assisted particle swarm optimization (PSO) algorithms for performing vector perturbation precoding, as well as for lowering the required transmission power at the base station (BS), while minimizing the expected average bit error ratio (BER) at the mobile terminals. We use the minimum BER criterion. We show that the novel quantum-assisted precoding methodology results in an enhanced BER performance, when compared with that of a classical methodology employing the PSO algorithm, while requiring the same computational complexity in the challenging rank-deficient scenarios, where the number of transmit antenna elements at the BS is lower than the number of users. Moreover, when there is limited channel state information feedback from the users to the BS, due to the necessary quantization of the channel states, the proposed quantum-assisted precoder outperforms the classical precoder.

INDEX TERMS Channel quantization, computational complexity, Dürr-Høyer algorithm, Grover's quantum search algorithm, multiuser transmission, orthogonal frequency division multiplexing, particle swarm optimization, quantum computing, vector perturbation.

LIST OF ABBREVIATIONS

AE	Antenna Element
AWGN	Additive White Gaussian Noise
BD	Block Diagonalization
BS	Base Station
CF	Cost Function
CFE	Cost Function Evaluation
CIR	Channel Impulse Response
CoMP	Coordinated Multi-Point
cPSO	continuous-valued Particle Swarm Optimization
cQPSO	continuous-valued Quantum-assisted Particle Swarm Optimization
CSI	Channel State Information
DHA	Dürr-Høyer Algorithm
dPSO	discrete-valued Particle Swarm Optimization
dQPSO	discrete-valued Quantum-assisted Particle Swarm Optimization
DS-CDMA	Direct Sequence - Code Division Multiple Access
EVA	Extended Vehicular A
FD-CHTF	Frequency-Domain CHannel Transfer Function
FDD	Frequency Division Duplexing
IDMA	Interleave Division Multiple Access
LLR	Log-Likelihood Ratios
MAP	Maximum *A Posteriori*
MBER	Minimum Bit Error Ratio
MC-IDMA	Multi-Carrier Interleave Division Multiple Access
MIMO	Multiple-Input Multiple-Output
MMSE	Minimum Mean Square Error
MUD	Multi-User Detection
MUT	Multi-User Transmission

NOMA	Non-Orthogonal Multiple Access
OFDMA	Orthogonal Frequency Division Multiple Access
OMA	Orthogonal Multiple Access
QPSK	Quadrature Phase Shift Keying
QPSO	Quantum-assisted Particle Swarm Optimization
QSA	Quantum Search Algorithms
SDMA	Spatial Division Multiple Access
SISO	Soft-Input Soft-Output
SNR	Signal to Noise Ratio
TDD	Time Division Duplexing
VP	Vector Perturbation
ZF	Zero Forcing

I. INTRODUCTION

In Orthogonal Multiple Access (OMA) systems, such as the traditional Direct Sequence - Code Division Multiple Access (DS-CDMA) [1], where each user has been allocated a unique, orthogonal spreading sequence, or in conventional Orthogonal Frequency Division Multiple Access (OFDMA) [2], where each user has been allocated a frequency band including multiple, but unique, orthogonal subcarriers, the search for a precoding matrix and the employment of vector perturbation is simple. The reason is that orthogonal multiple access systems are usually under-loaded systems, since the number of transmit Antenna Elements (AE) at the Base Station (BS) is typically higher than the number of receive AEs at the single user supported on a specific frequency, time or code resource element. Due to this fact, the employment of linear precoding techniques at the BS leads to satisfactory performance.

Orthogonal multiple access systems exhibit limited throughput, since different users are not allowed to share the same resources. The concept of Non-Orthogonal Multiple Access (NOMA) systems [3]–[5] allows more users to be served at the same time, while using the same resources, resulting in an increased normalized system throughput. Examples of NOMA systems include specific OFDMA arrangements, which allow multiple users to simultaneously activate the same subcarriers [6], [7] and Spatial Division Multiple Access (SDMA) systems, where the users are separated based on their spatial signature [8]. Furthermore, classic DS-CDMA systems relying on non-orthogonal m-sequence spreading codes, or Interleave Division Multiple Access (IDMA) systems, where the users are separated according to their unique interleaving sequences [9]–[11] also belong to the family of NOMA systems. However, more sophisticated signal processing techniques may have to be adopted both in the uplink and downlink of NOMA systems, for signal detection or signal preprocessing, respectively, since the resultant systems may be rank-deficient, because the number of AEs at the BS may be lower than the sum of AEs of all users that simultaneously share the same resources.

In this contribution, we focus our attention on the downlink of a communications system, where the BS has to convey information to the users supported. The BS preprocesses each user's symbols, based on the number of transmit AEs and on the Channel State Information (CSI) between a transmit AE at the BS and a receive AE of a user. The Multi-User Transmission (MUT) regime of the downlink may be considered as the counterpart of Multi-User Detection (MUD) in the uplink [12]. When Time Division Duplexing (TDD) is used, the same frequency band is exploited for both the uplink and the downlink communication between the BS and the users, while the uplink and the downlink are separated by having been allocated different time slots. Therefore, the BS may estimate the CSI of all the required channels that will be used for the downlink. On the other hand, when Frequency Division Duplexing (FDD) is used, different frequency bands are allocated for the uplink and downlink. Since in this case the BS is unable to estimate the CSI, the users have to transmit the estimated CSI of the downlink back to the BS through feedback channels. In [13] generalized Zero Forcing (ZF) and Minimum Mean-Square Error (MMSE) channel inversion algorithms are proposed for multi-user Multiple-Input Multiple-Output (MIMO) systems, in order to compensate for the degraded performance of the Block Diagonalization (BD) technique in imperfect channel estimation scenarios. However, linear preprocessing methods invoked for rank-deficient systems exhibit a degraded performance, necessitating the employment of sophisticated non-linear algorithms. Spreading codes may be allocated to the users for exploiting the multiple access interference [14], [15]. Other downlink precoders, which exploit the interference between the downlink users for enhancing the Signal to Interference-plus-Noise Ratio (SINR) at the users supported in non-orthognal systems have been proposed in [16]–[20].

In [21], the continuous-valued Particle Swarm Optimization (cPSO) algorithm was employed for finding the optimal precoding matrix, based on the Minimum Bit Error Ratio (MBER) criterion. A discrete-valued PSO (dPSO) algorithm was employed in the context of Vector Perturbation (VP) [22]–[28] in [29], for finding the optimal MBER vector for perturbing the symbol vector, while keeping the transmission power under a certain threshold. The same authors in [30] proposed a preprocessing methodology, where a dPSO is initially used for VP given a precoding matrix found with the aid of linear ZF or MMSE methods. Having obtained the perturbation vector, a cPSO is employed for fine-tuning the perturbed and preprocessed vector, again in terms of the MBER criterion, while satisfying the transmission power constraint. Table 1 summarizes selected contributions in the field of multi-user transmission preprocessing with the aid of vector perturbation.

With Moore's law expected to enter the quantum domain in 2017 [31], research focusing on creating a universal quantum computer has intensified. Quantum computing [32]–[34] is expected to replace specific technological applications. In this treatise, we focus on the employment of

TABLE 1. Selected contributions in vector perturbation - aided multi-user transmission.

Year	Author(s)	Contribution
2005	Peel *et al.* [22], [23]	Proposed the vector perturbation precoding technique for the downlink of multi-user systems. A sphere encoder was used for selecting a suitable vector for perturbing the data, while minimizing the transmission power.
2008	Chae *et al.* [24]	Presented a joint block diagonalization and vector perturbation multi-user downlink technique for reducing the receivers' complexity.
2009	Yao *et al.* [21]	Developed a continuous-valued particle swarm optimization algorithm for finding the optimal precoding matrix relying on the minimum bit error ratio criterion.
	Yao *et al.* [29]	Proposed a discrete-valued particle swarm optimization algorithm for searching for the specific perturbation vector that minimizes the system's average bit error ratio.
2011	Park *et al.* [25]	Suggested a low-complexity algorithm for vector perturbation, which includes iterative independent searches for the real and imaginary parts of the perturbation vector.
	Yao *et al.* [30]	Proposed the employment of a continuous-valued particle swarm optimization algorithm for directly searching for the specific transmission vector, which includes both the precoding matrix and the vector perturbation along with the data vector, that minimizes the bit error ratio criterion, rather than performing independent searches.
2013	Masouros *et al.* [26]	Developed a low-complexity vector perturbation methodology relying on a sphere search for the minimization of the transmission power with the aid of a threshold weight, which, when met, terminates the search earlier.
2014	Masouros *et al.* [27]	Proposed a vector perturbation algorithm suitable for the downlink of multi-user systems with limited feedback, where the users have no access to the scaling factor and the - otherwise necessary - modulo operation is not performed at the receivers.
2015	Herath *et al.* [28]	Proposed a vector perturbation precoding methodology for employment in the downlink of Coordinated Multi-Point (CoMP) multi-user systems.

Quantum Search Algorithms (QSA) [35] in a MUT application. Grover's QSA [36], [37] succeeds in finding a specific entry in an unsorted database of size N with $\sim$100% probability of success, by querying the database $O(\sqrt{N})$ times, as long as the number of times the searched entry appears in the database is known. Boyer *et al.* improved Grover's QSA in [38], by proposing an algorithm that finds the specific entry in a database after $O(\sqrt{N})$ queries, even when the number of times the entry is included in the database is unknown. Moreover, Dürr and Høyer in [39] presented a QSA for finding the minimum entry in a database after $O(\sqrt{N})$ queries, without any other prior knowledge, except for the database's size. In [8], we proposed a method for reducing the complexity of the Dürr-Høyer Algorithm (DHA), solely based on the database's size and the algorithm's statistics, which may be obtained offline. In [7], [8], [11], and [40], we have presented quantum-assisted multi-user detectors based on the DHA and we have employed them in the uplink of wireless communications systems for performing optimal coherent and non-coherent hard-input hard-output quantum-assisted MUD, as well as soft-input soft-output quantum-assisted MUD.

Against this background, our novel contributions are:

1) *We propose a heuristic Quantum-assisted Particle Swarm Optimization (QPSO) algorithm, by incorporating the DHA in the cost function evaluation process of each generation. We show the suitability of the QPSO for conducting search both in discrete-valued, as well as in continuous-valued search spaces.*
2) *We employ the QPSO in the context of MUT and we conclude that the QPSO achieves better performance than the PSO for the same complexity. Similarly, we demonstrate that the QPSO achieves equivalent performance to the PSO, while requiring lower computational complexity. The discrete-valued QPSO (dQPSO) may replace the dPSO in the VP search, while the continuous-valued QPSO (cQPSO) may be used instead of the cPSO for either improving the achievable performance, or for reducing the complexity.*
3) *We use the MBER criterion for optimizing the preprocessed transmitted signal in the downlink of a NOMA system. More precisely, we investigate a rank-deficient Multi-Carrier IDMA (MC-IDMA) system, where multiple users are allowed to share the same subcarriers during the same time slots, while each user's data is interleaved with the aid of a different interleaving sequence. The powerful MBER criterion [41]–[43] uses a more complex cost function than the MMSE criterion, hence requiring the powerful parallel search technique conceived in this treatise. At the same time, it yields an improved performance, since it directly leads to the multi-level vector that minimizes the BER instead of the mean square error [21], [44], [45].*
4) *When FDD is used, the mobile users send quantized versions of the estimated CSI to the BS. The impact that erroneous and quantized CSI availability at the base station has on VP precoding has been studied in [46]–[48]. Assuming perfect channel estimation and noiseless feedback channels, we investigate the effect that the precision of the quantization has in our proposed quantum-assisted MUT algorithm.*

The paper is structured as described in Fig. 1. In Section II, we analyse the downlink of the NOMA system, including the

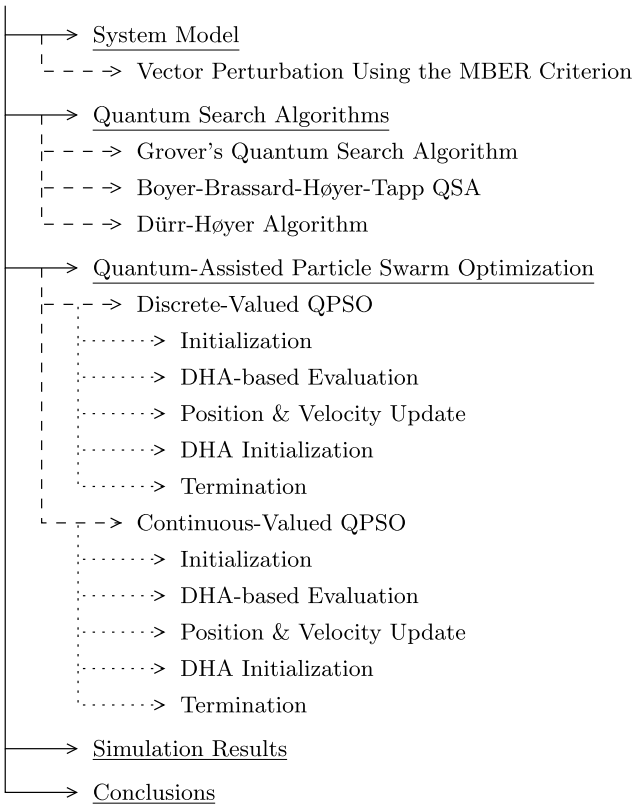

FIGURE 1. Summary of the sections of the paper.

MUT process at the BS, as well as the channel quantization at the mobile terminals. In Section III, we state the prerequisites of quantum computing and briefly introduce the quantum search algorithms that are employed in the proposed QPSO, which is explored in Section IV. The simulation results of using the QPSO for operating the MUT scheme are discussed in Section V. Finally, our conclusions are offered in Section VI.

II. SYSTEM MODEL

The downlink of a MC-IDMA system supporting U users is depicted in Fig. 2. The BS encodes the information bits of each user $\{b_u\}$, for $u \in \{1, 2, \ldots, U\}$, using a turbo convolutional code, before interleaving the encoded bit streams $\{c_u\}$ using user-specific interleaving sequences. The encoded and interleaved bits $\{i_u\}$ are then mapped to Quadrature Phase Shift Keying (QPSK) symbols, forming the symbol streams $\{x_u\}$.

For simplicity, let us interpret the MUT as the dual counterpart of an MUD. Explicitly, when a pair of QPSK users transmit in the uplink, the MUD may consider all 16 2-user symbols for jointly detecting their signals. Can we now view the downlink MUT problem as the transmission of a specific 16-ary symbol, so that each of the two downlink receivers can recover its intended signal after some low-complexity manipulations? The answer is a resounding "yes". Let us hence explore this in more detail.

The vector precoder of Fig. 2 maps the users' symbols to the signals to be transmitted by the N_T transmit antennas of the BS, while also taking into account the effect of the fading channel imposed on the received signals at each user's terminal. By predicting and then carrying out the inverse of these applications at the BS, most of the complexity that would have been required by the detection stages of each user is shifted to the BS's side. The vector precoding technique, which is adopted in the downlink, may be employed in any NOMA multiple-access scheme. In our contribution we opted for a special case of MC-IDMA, by employing the unique interleaving sequences per user, but without including an additional repetition code for increasing the length of the bit sequence. The only difference between the employed system and an SDMA-OFDM system is that the interleaving sequences are user-specific.

In the MC-IDMA system investigated, vector precoding takes place on a per subcarrier basis. When assuming Q available orthogonal subcarriers and that all users transmit on all subcarriers, the MC-IDMA system may be described as a NOMA system, where the users are separated in the spatial domain based on their Channel Impulse Responses (CIR). On the qth subcarrier, with $q \in \{1, 2, \ldots, Q\}$, the vector precoder has to determine the $(N_T \times 1)$-element vector $\mathbf{d}_q$, based on the $(U \times 1)$-element vector $\mathbf{x}_q$, which includes the symbols that have to be conveyed to their corresponding users on the qth subcarrier, as well as on the $(U \times N_T)$-element Frequency-Domain CHannel Transfer Function (FD-CHTF) matrix of the qth subcarrier $\mathbf{H}_q$. The CIRs are either estimated at the BS if TDD is used, or estimated at and fed back by the users if FDD is used. From this point onwards, let us omit the subscript q, by simply mentioning that the same procedure is followed on all Q subcarriers. The signal vector $\mathbf{d}$ is constructed by the vector precoder as in

$$\mathbf{d} = \mathbf{P} \cdot (\mathbf{x} + \mathbf{w}), \tag{1}$$

where the $(N_T \times U)$-element matrix $\mathbf{P}$ is the precoding matrix, which may be efficiently computed using the conventional ZF or the MMSE precoders, while the $(U \times 1)$-element vector $\mathbf{x}$ includes the users' symbols and the $(U \times 1)$-element vector $\mathbf{w}$ is the discrete perturbation vector, which is appropriately selected for minimizing the optimization criterion, such as the BER or the MSE, while satisfying the maximum transmission power constraint.

Initially in our proposed methodology, the precoding matrix $\mathbf{P}$ is found based on the MMSE criterion, as encapsulated in

$$\mathbf{P} = \mathbf{H}^H \left(\mathbf{H}\mathbf{H}^H + \sigma_n^2 \mathbf{I}_U \right)^{-1}, \tag{2}$$

where σ_n^2 is the Additive White Gaussian Noise's (AWGN) variance at the users' receive antennas and $\mathbf{I}_U$ is the $(U \times U)$-element identity matrix. In our simulations, we have assumed a normalized transmission power of $E_T = 1$, hence the average Signal to Noise Ratio (SNR) is equal to $\text{SNR} = 1/\sigma_n^2$. In lightly loaded, or full-rank systems,

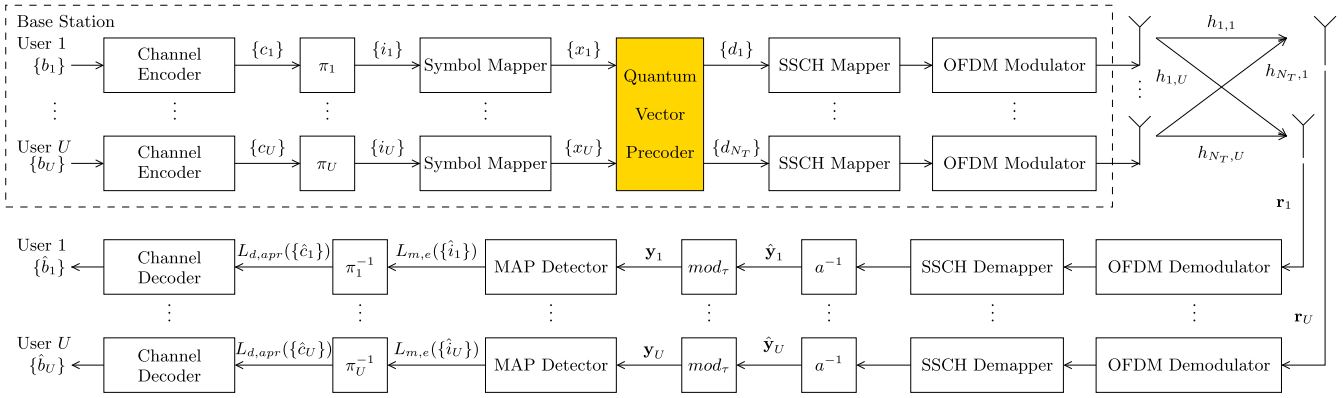

FIGURE 2. Downlink of MC-IDMA communication system's block diagram supporting U single-antenna users employing turbo convolutional coding and multi-user transmission precoding with the aid of vector perturbation.

where we have $N_T \geq U$, simply substituting the precoding matrix of (2) into (1), while setting $\mathbf{w}$ equal to the $(U \times 1)$-element zero vector would result in a satisfactory performance. However, in the rank-deficient systems investigated, where $N_T < U$, applying the same methodology would result in a degraded performance. Nevertheless, we may employ the calculation of the precoding matrix as the first step of the vector precoding process and based on this we may proceed by computing the perturbation vector $\mathbf{w}$ of (1).

Let us consider a tutorial example, by investigating the downlink a rank-deficient system having a BS with $N_T = 2$ transmit AEs supporting $U = 4$ users. Let us also assume that the four QPSK symbols that have to be conveyed to the four users over the first subcarrier are

$$\mathbf{x}_{ex} = \begin{bmatrix} 0.71 - j \cdot 0.71 \\ 0.71 - j \cdot 0.71 \\ -0.71 + j \cdot 0.71 \\ -0.71 + j \cdot 0.71 \end{bmatrix} \tag{3}$$

and that the frequency-domain channel states between the $N_T = 2$ transmit AEs and the $U = 4$ users are

$$\mathbf{H}_{ex} = \begin{bmatrix} 0.52 + j \cdot 1.87 & 0.93 + j \cdot 0.16 \\ -0.54 - j \cdot 0.38 & -0.51 - j \cdot 0.10 \\ -0.33 - j \cdot 0.61 & 0.02 - j \cdot 0.72 \\ -1.46 + j \cdot 0.80 & -0.14 - j \cdot 1.01 \end{bmatrix}. \tag{4}$$

Based on (4) and on (2) and assuming an SNR of 10 dB, we have $\sigma_n^2 = 0.1$ and hence the precoding matrix becomes

$$\mathbf{P}_{ex} = \begin{bmatrix} 0.03 - j \cdot 0.25 & 0.33 + j \cdot 0.03 \\ -0.05 + j \cdot 0.049 & -0.16 + j \cdot 0.019 \\ -0.04 + j \cdot 0.05 & 0.02 + j \cdot 0.24 \\ -0.19 - j \cdot 0.16 & 0.017 + j \cdot 0.41 \end{bmatrix}^T. \tag{5}$$

If we do not employ a perturbation vector, which corresponds to $\mathbf{w} = [0, 0, 0, 0]^T$, then the signals transmitted by the transmit AEs are

$$\mathbf{d}_{ex,\mathbf{w}=\{0\}^U} = \mathbf{P}_{ex} \cdot \mathbf{x}_{ex} = \begin{bmatrix} 0.08 - j \cdot 0.22 \\ -0.34 - j \cdot 0.51 \end{bmatrix}, \tag{6}$$

with an associated transmit power of $\|\mathbf{d}_{ex,\mathbf{w}=\{0\}^U}\|^2 = 0.43$.

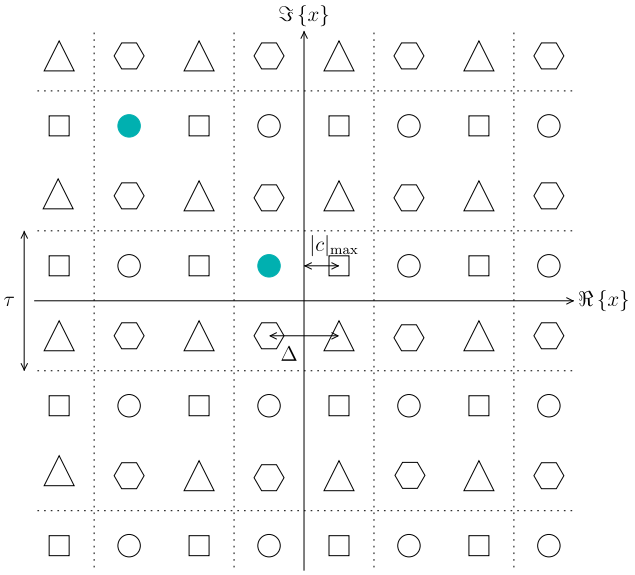

FIGURE 3. The resultant legitimate constellation, after applying a perturbation vector. As an example, the specific symbol represented by the filled circle of the original QPSK constellation, which is the closest to the origin, would be transmitted without a perturbation vector. When that symbol is subjected to the perturbation vector $\mathbf{w} = -1 + j$, the top left filled circle will be transmitted instead for the sake of minimizing the interference at the receiver.

In this contribution, we will search for the optimal discrete perturbation vector $\mathbf{w}$ based on the MBER criterion, while taking into consideration the transmission power constraint. The discrete perturbation vector maps a symbol from the original constellation to the same symbol location of a shifted constellation, as demonstrated in Fig. 3, which illustrates a periodical replication of the original QPSK constellation. The uth element of the perturbation vector belongs to

$$w_u = \alpha_u \cdot \tau + j \cdot \beta_u \cdot \tau, \tag{7}$$

where a_u and b_u are integers for $u \in \{1, 2, \ldots U\}$ and τ is a positive real number, which depends on the originally selected constellation. Based on [23], τ may be

calculated as in

$$\tau = 2\,|c|_{\max} + \Delta, \tag{8}$$

where $|c|_{\max}$ is the one-dimensional amplitude of the original constellation's symbol that has the maximum magnitude, while Δ is the distance between the closest neighbouring symbols of the original constellation. For example, when QPSK associated with $x_u = \pm 1/\sqrt{2} \pm j/\sqrt{2}$ is used, we have $|c|_{\max} = 1/\sqrt{2}$ and $\Delta = \sqrt{2}$, yielding $\tau = 2 \cdot \sqrt{2}$ according to (8).

In our tutorial example, the optimal discrete perturbation vector $\mathbf{w}$ found by using the dPSO algorithm based on the MBER criterion is

$$\mathbf{w}_{ex} = \begin{bmatrix} \alpha_1 + j \cdot \beta_1 \\ \alpha_2 + j \cdot \beta_2 \\ \alpha_3 + j \cdot \beta_3 \\ \alpha_4 + j \cdot \beta_4 \end{bmatrix} \cdot \tau = \begin{bmatrix} -1 + j \cdot 0 \\ 0 + j \cdot 0 \\ 1 + j \cdot 0 \\ 1 - j \cdot 1 \end{bmatrix} \cdot 2.83. \tag{9}$$

The perturbed signal vector $(\mathbf{x}_{ex} + \mathbf{w}_{ex})$ may be interpreted as four superimposed symbols of Fig. 3; one for each user supported in the system. By using the perturbation vector of (9), the resultant transmitted signals are

$$\mathbf{d}_{ex} = \mathbf{P}_{ex} \cdot (\mathbf{x}_{ex} + \mathbf{w}_{ex}) = \begin{bmatrix} -1.11 + j \cdot 0.74 \\ 0.003 - j \cdot 1.19 \end{bmatrix}, \tag{10}$$

with an associated transmission power of $\|\mathbf{d}_{ex}\|^2 = 3.22$.

Having calculated the precoding matrix $\mathbf{P}$ and selected the appropriate perturbation vector $\mathbf{w}$ as analysed in Section II-A, the signal vector $\mathbf{d}$ of (1) is transmitted to the users. On a per subcarrier basis, the $(U \times 1)$-element signal vector received at the U mobile users $\hat{\mathbf{y}} = \left[\hat{y}_1, \ldots, \hat{y}_U\right]^T$ becomes

$$\hat{\mathbf{y}} = \mathbf{H} \cdot \mathbf{d} + a^{-1}\mathbf{n}, \tag{11}$$

where the $(U \times 1)$-element vector $\mathbf{n}$ represents the AWGN at the users' receive antennas and a is a scalar parameter chosen as a function of the transmitted signal's power $\|\mathbf{d}\|^2$ and the affordable maximum transmitted power E_T, as encapsulated in

$$a = \sqrt{\frac{E_T}{\|\mathbf{d}\|^2}}. \tag{12}$$

Even though the scaling factor a is applied at the BS before transmission, we may model the system as if the transmission power is equal to $\|\mathbf{d}\|^2$ and the noise power varies depending on a, as described in (11). In our simulations we consider $E_T = 1$.

Returning to our scenario, the received signals at the $U = 4$ users, if $\mathbf{d}_{ex,\mathbf{w}=\{0\}^U}$ was transmitted, would be

$$\begin{aligned} \hat{\mathbf{y}}_{ex,\mathbf{w}=\{0\}^U} &= \mathbf{H}_{ex} \cdot \mathbf{d}_{ex,\mathbf{w}=\{0\}^U} + \alpha^{-1}_{ex,\mathbf{w}=\{0\}^U} \cdot \mathbf{n}_{ex} \\ &= \begin{bmatrix} 0.12 - j \cdot 0.32 \\ -0.15 + j \cdot 0.33 \\ -0.62 + j \cdot 0.23 \\ -0.41 + j \cdot 1.03 \end{bmatrix}, \end{aligned} \tag{13}$$

where $\alpha^{-1}_{ex,\mathbf{w}=\{0\}^U} = \sqrt{\|\mathbf{d}_{ex,\mathbf{w}=\{0\}^U}\|^2} = 0.66$ and

$$\mathbf{n}_{ex} = \begin{bmatrix} -0.16 + j \cdot 0.26 \\ -0.22 - j \cdot 0.08 \\ -0.12 - j \cdot 0.04 \\ 0.007 + j \cdot 0.34 \end{bmatrix} \tag{14}$$

were used. On the other hand, if $\mathbf{d}_{ex}$ was transmitted instead, the received signals would be

$$\hat{\mathbf{y}}_{ex} = \mathbf{H}_{ex} \cdot \mathbf{d}_{ex} + \alpha^{-1}_{ex} \cdot \mathbf{n}_{ex} = \begin{bmatrix} -2.44 - j \cdot 0.11 \\ 0.61 - j \cdot 0.73 \\ 1.47 + j \cdot 0.39 \\ 2.25 - j \cdot 1.53 \end{bmatrix}, \tag{15}$$

where $\alpha^{-1}_{ex} = \sqrt{\|\mathbf{d}_{ex}\|^2} = 1.79$ and the noise vector of (14) were used.

Then, a modulo-τ operation is performed upon each received signal, as illustrated in Fig. 2. The modulo-τ operation is used for mapping the received symbol of the shifted constellation modified by the perturbation vector of the BS, to its corresponding position in the original constellation, effectively performing the inverse operation of Fig. 3. The modulo-τ operation carried out at the uth user results in the signal y_u, as stated in

$$\begin{aligned} y_u &= mod_\tau\left(\hat{y}_u\right) \\ &= \hat{y}_u - \left\lfloor \frac{\Re\left\{\hat{y}_u\right\} + \tau/2}{\tau} \right\rfloor \tau - j \left\lfloor \frac{\Im\left\{\hat{y}_u\right\} + \tau/2}{\tau} \right\rfloor \tau. \end{aligned} \tag{16}$$

Let us now further process the received signals in the two scenarios of our tutorial example. According to (16), if no perturbation vector was used and hence $\hat{\mathbf{y}}_{ex,\mathbf{w}=\{0\}^U}$ of (13) was received by the users, then we would have

$$\mathbf{y}_{ex,\mathbf{w}=\{0\}^U} = \hat{\mathbf{y}}_{ex,\mathbf{w}=\{0\}^U} = \begin{bmatrix} 0.12 - j \cdot 0.32 \\ -0.15 + j \cdot 0.33 \\ -0.62 + j \cdot 0.23 \\ -0.41 + j \cdot 1.03 \end{bmatrix}. \tag{17}$$

By employing hard detection at each user's terminal, the detected symbols would be

$$\hat{\mathbf{x}}_{ex,\mathbf{w}=\{0\}^U} = \begin{bmatrix} 0.71 - j \cdot 0.71 \\ -0.71 + j \cdot 0.71 \\ -0.71 + j \cdot 0.71 \\ -0.71 + j \cdot 0.71 \end{bmatrix}, \tag{18}$$

resulting in a symbol error for the second user, when compared to the information symbols of (3). However, if the perturbation vector of (9) was applied, the received signal after the modulo-τ operation of (16) would be equal to

$$\mathbf{y}_{ex} = \begin{bmatrix} 0.39 - j \cdot 0.11 \\ 0.61 - j \cdot 0.73 \\ -1.36 + j \cdot 0.39 \\ -0.58 + j \cdot 1.30 \end{bmatrix}, \tag{19}$$

resulting in an error-free symbol detection of

$$\hat{\mathbf{x}}_{ex} = \begin{bmatrix} 0.71 - j \cdot 0.71 \\ 0.71 - j \cdot 0.71 \\ -0.71 + j \cdot 0.71 \\ -0.71 + j \cdot 0.71 \end{bmatrix}. \tag{20}$$

In this contribution, the Soft-Input Soft-Output (SISO) Maximum *A Posteriori* probability (MAP) detector [2] is employed at each user, as seen in Fig. 2. The MAP detector performs soft symbol detection on a per subcarrier basis, which yields the bit-based Log-Likelihood Ratios (LLR). Focusing on the uth user's mth bit on the qth subcarrier, its *a posteriori* LLR $L_{m,po}\left(b_u^{(m)}\right)$ may be described as

$$L_{m,po}\left(b_u^{(m)}\right) = \ln \frac{\sum\limits_{x \in \chi(m,0)} P\left(y_u|x\right) P(x)}{\sum\limits_{x \in \chi(m,1)} P\left(y_u|x\right) P(x)}, \tag{21}$$

where $\chi(m, \mathrm{v})$ represents the specific symbols of the original constellation for which the mth bit is equal to v, $P(x)$ is the *a priori* probability of the symbol x and $P(y_u|x)$ is the probability of obtaining y_u, given that x was transmitted, which may be formulated as

$$P(y_u|x) = \frac{1}{a^{-1}\sigma_n\sqrt{2\pi}} \exp\left(-\frac{\|y_u - x\|^2}{2\sigma_n^2 a^{-2}}\right), \tag{22}$$

where the $2\sigma_n^2 a^{-2}$ is the effective noise variance. The extrinsic LLRs $L_{m,e}\left(b_u^{(m)}\right)$ are then fed to the deinterleaver, after being calculated as in

$$L_{m,e}\left(b_u^{(m)}\right) = L_{m,po}\left(b_u^{(m)}\right) - \ln \frac{P\left(b_u^{(m)} = 0\right)}{P\left(b_u^{(m)} = 1\right)}. \tag{23}$$

In our investigated systems, the transmitted bits are equiprobable, therefore we have $P\left(b_u^{(m)} = 0\right) = P\left(b_u^{(m)} = 1\right) = 0.5$ and hence $L_{m,e}\left(b_u^{(m)}\right) = L_{m,po}\left(b_u^{(m)}\right)$. Once the extrinsic LLRs have been deinterleaved, the resultant *a priori* LLRs are fed into the turbo decoders. The estimated information bits of each user are obtained by performing a hard decision at the output LLRs of the decoders in Fig. 2.

A. VECTOR PERTURBATION USING THE MBER CRITERION

The analytical BER functions differ, depending on the modulation scheme selected. Let us analyse the vector perturbation process of finding $\mathbf{d}$ of (1), relying on the QPSK modulation scheme, since this is used in our simulation results. It should be noted that the methodology is the same for all modulation schemes, when the corresponding functions of error probability are used. Let us initially focus our attention on the uth user's symbol and again, omit the subcarrier's subscript. The error probability for the in-phase component after the modulo-τ operation of (16), when a vector $\mathbf{d}$ is transmitted by the BS's transmit antennas, becomes equal to [30]

$$\begin{aligned} P_{e,I,u}\left(\mathbf{d}\right) \approx\ & Q\left(\frac{c_R^{(u)} + 3\tau}{a^{-1}\sigma_n}\right) + Q\left(\frac{-\frac{5}{2}\tau - c_R^{(u)}}{a^{-1}\sigma_n}\right) \\ & - Q\left(\frac{-2\tau - c_R^{(u)}}{a^{-1}\sigma_n}\right) + Q\left(\frac{-\frac{3}{2}\tau - c_R^{(u)}}{a^{-1}\sigma_n}\right) \\ & - Q\left(\frac{-\tau - c_R^{(u)}}{a^{-1}\sigma_n}\right) + Q\left(\frac{-\frac{1}{2}\tau - c_R^{(u)}}{a^{-1}\sigma_n}\right) \\ & - Q\left(\frac{-c_R^{(u)}}{a^{-1}\sigma_n}\right) + Q\left(\frac{\frac{1}{2}\tau - c_R^{(u)}}{a^{-1}\sigma_n}\right) \\ & - Q\left(\frac{\tau - c_R^{(u)}}{a^{-1}\sigma_n}\right) + Q\left(\frac{\frac{3}{2}\tau - c_R^{(u)}}{a^{-1}\sigma_n}\right) \\ & - Q\left(\frac{2\tau - c_R^{(u)}}{a^{-1}\sigma_n}\right) + Q\left(\frac{\frac{5}{2}\tau - c_R^{(u)}}{a^{-1}\sigma_n}\right) \\ & - Q\left(\frac{3\tau - c_R^{(u)}}{a^{-1}\sigma_n}\right), \end{aligned} \tag{24}$$

where $Q(\cdot)$ is the tail probability of the normal distribution and the user-specific $c_R^{(u)}$ is a function of $\mathbf{d}$, representing the mean value of the variable $\left(\mathrm{sign}\left(\Re\left\{x_u\right\}\right)\Re\left\{\hat{y}_u\right\}\right)$, as encapsulated in

$$c_R^{(u)} = \mathrm{sign}\left(\Re\left\{x_u\right\}\right)\Re\left\{\mathbf{h}_u\mathbf{d}\right\}, \tag{25}$$

where $\mathbf{h}_u$ is the uth row of the qth subcarrier's FD-CHTF matrix $\mathbf{H}$. The error probability $P_{e,Q,u}(\mathbf{d})$ of the uth user's quadrature-phase bit is the same as in (24), we just replace $c_R^{(u)}$ by $c_I^{(u)}$, which may be formulated as

$$c_I^{(u)} = \mathrm{sign}\left(\Im\left\{x_u\right\}\right)\Im\left\{\mathbf{h}_u\mathbf{d}\right\}. \tag{26}$$

By combining (24) for the in-phase and quadrature-phase components, the average BER of the uth user becomes equal to

$$P_{e,u}(\mathbf{d}) = \frac{P_{e,I,u}(\mathbf{d}) + P_{e,Q,u}(\mathbf{d})}{2}. \tag{27}$$

Finally, the average BER of all users, as a function of the transmitted signal $\mathbf{d}$ is encapsulated in

$$P_e(\mathbf{d}) = \frac{1}{U}\sum_{u=1}^{U} P_{e,u}(\mathbf{d}). \tag{28}$$

The error probability of (28) may be considered as the Cost Function (CF) of the search for the discrete- and complex-valued perturbation vector $\mathbf{w}$, given the precoding matrix $\mathbf{P}$, since that search is performed with the goal of minimizing the total average error probability of (28). In other words, the search aims for finding the optimal transmission vector $\mathbf{d}_{opt}$, which minimizes the error probability of (28), as stated in [30]

$$\mathbf{d}_{opt} = \arg\min_{\mathbf{d}}\left[P_e\left(\mathbf{d}\right)\right]. \tag{29}$$

More specifically, having calculated the precoding matrix $\mathbf{P}$ by using the MMSE criterion, we perform

a discrete- and complex-valued search by using the proposed DHA-aided dPSO algorithm for finding the optimal MBER perturbation vector $\mathbf{w}$ of (1), which minimizes the MBER metric of (28). The output transmission vector $\mathbf{d}$ of that search will then be used as an initial input for a subsequent continuous- and complex-valued search for $\mathbf{d}$ of (1) by using the proposed DHA-aided cPSO algorithm, again based on the MBER criterion of (28). The aim of the second search is to "fine tune" the output of the discrete search within its neighbourhood, with the discrete search being the most crucial one for optimizing the system's performance, as it is exemplified in Section V. Since the search space of $\mathbf{w} = [w_1, \ldots, w_U]^T$ is infinite, we will limit the search space to $\Re\{w_u\} \in \{-2, -1, 0, 1, 2\}$ and $\Im\{w_u\} \in \{-2, -1, 0, 1, 2\}$, which - based on our statistical simulations - includes ∼100% of the cases.

It should be noted here that any modulation scheme may be used in conjunction with VP based on the MBER criterion, as long as its associated MBER function is used as a cost function, since (24) corresponds to the QPSK modulation. Our proposed quantum-assisted algorithm may also be used in conjunction with any modulation scheme. The motivation behind opting for QPSK in our paper is the ease of presentation and simulation complexity due to the naturally high complexity required for simulating quantum algorithms on classical computers.

III. QUANTUM SEARCH ALGORITHMS

Contrary to classical computing, where a bit may only assume the values 0 or 1, a quantum bit [32], or *qubit*[1], $|q\rangle$ in quantum computing may be found in a superposition of the states $|0\rangle$ or $|1\rangle$, as in $|q\rangle = \alpha|0\rangle + \beta|1\rangle$, where $\alpha, \beta \in \mathbb{C}$ and $|\alpha|^2 + |\beta|^2 = 1$. When a qubit is *measured*, or *observed*, in the computational basis [32] $\{|0\rangle, |1\rangle\}$, then the probability of obtaining $|q\rangle = |0\rangle$ is $|\alpha|^2$, while that of observing $|q\rangle = |1\rangle$ is $|\beta|^2$. A qubit's state is evolved by using unitary operators. For example, the Hadamard gate H is a unitary operator, which carries out the mapping of $H|0\rangle = |+\rangle = (|0\rangle + |1\rangle)/\sqrt{2}$ and $H|1\rangle = |-\rangle = (|0\rangle - |1\rangle)/\sqrt{2}$. By employing multiple qubits, we may create quantum registers. For instance, by using two qubits initially at the zero state $|q_1\rangle|q_2\rangle = |00\rangle$ and Hadamard operators, we may create an equiprobable superposition of four states $H|q_2\rangle \otimes H|q_2\rangle = (|0\rangle+|1\rangle)/\sqrt{2} \otimes (|0\rangle+|1\rangle)/\sqrt{2} = (|00\rangle+|01\rangle+|10\rangle+|11\rangle)/2$. If the states of two or more qubits cannot be described separately, as in the aforementioned equiprobable superposition of states, these qubits are termed as *entangled* qubits. Two qubits in the Bell state [32] $(|00\rangle+|11\rangle)/\sqrt{2}$ form an example of quantum entanglement.

A. GROVER's QUANTUM SEARCH ALGORITHM

Grover's QSA [36], [37] succeeds in finding the address x of a desired entry δ in an N-sized database f, so that $f(x) = \delta$, with ∼100% success probability after as few as $O(\sqrt{N})$ queries in the database, while the optimal brute-force search requires $O(N)$ Cost Function Evaluations (CFE). Grover's QSA initially prepares an equiprobable superposition of N states, by employing $n = \log_2 N$ qubits, as in

$$|\psi_1\rangle = \frac{1}{\sqrt{N}} \left(\sum_{x=0}^{N} |x\rangle \right) |0\rangle^{\otimes \Phi}, \tag{30}$$

where the first n qubits represent the *index register* and the last Φ number of qubits form the *value register*. The value register, initially in the all-zero state $|0\rangle^{\otimes\Phi}$, will contain the CF values of all x inputs simultaneously, while being entangled to their respective input value of the index register, after a single operation of a unitary U_f gate [49]. The U_f gate receives as inputs both the index register, as well as the value register, and evaluates the CF $f(x)$ of (28), entangling the qubits of the index register to those of the value register. In our scenarios, $f(x)$ is equal to $P_e(\mathbf{d})$ of (28), where the relationship between x and $\mathbf{d}$ or the associated perturbation vector $\mathbf{w}$ may also be specifically arranged for ensuring that x acts as the increasing index of the vector $\mathbf{d}$ or $\mathbf{w}$, as it will be further analysed in Section IV, where the QPSO is investigated. After a single application of the U_f gate, the quantum system will be in the following superposition of states

$$|\psi_{1,\,U_f}\rangle = \frac{1}{\sqrt{N}} \sum_{x=0}^{N} |x\rangle |f(x)\rangle, \tag{31}$$

where a potential observation of the n-qubit *index register* $|i\rangle$ will also yield the corresponding CF value as the content of the Φ-qubit value register.

Grover's QSA then employs a unitary operator termed as the Oracle O, which is a quantum bit string comparator [50] conceived for checking whether a specific combination of Φ qubits in the value register is equal to the desired entry δ.[2] The Oracle flips the sign of the specific quantum state in the index register, which has a CF value equal to δ, with the aid of another auxiliary qubit initially found in the $|-\rangle$ state [36]. After the operation of the Oracle, the diffusion operator, which consists of three unitary operators $D = HP_0H$ is applied to the index register. The gate P_0 flips the amplitude's sign of all quantum states, except for the all-zero state. The effect that the diffusion operator has on the index register is that it reflects the amplitudes of all its states with respect to their average amplitude after the operation of the Oracle.

The operation of the Oracle O, followed by the diffusion operator D describes the Grover operator $\mathcal{G} = D \cdot O$. The Grover operator is applied to the equiprobable superposition of states $L_{opt} = \left\lfloor \frac{\pi}{4}\sqrt{\frac{N}{S}} \right\rfloor$ number of times, which is necessary for ∼100% success probability [38] with S representing the number of times that δ appears in the database and hence

[1]For an extensive tutorial on quantum computing and quantum search algorithms employed in wireless communications, please refer to [35].

[2]The value of δ is also created by using Φ qubits, without them being in a superposition of states, since δ is a known scalar value.

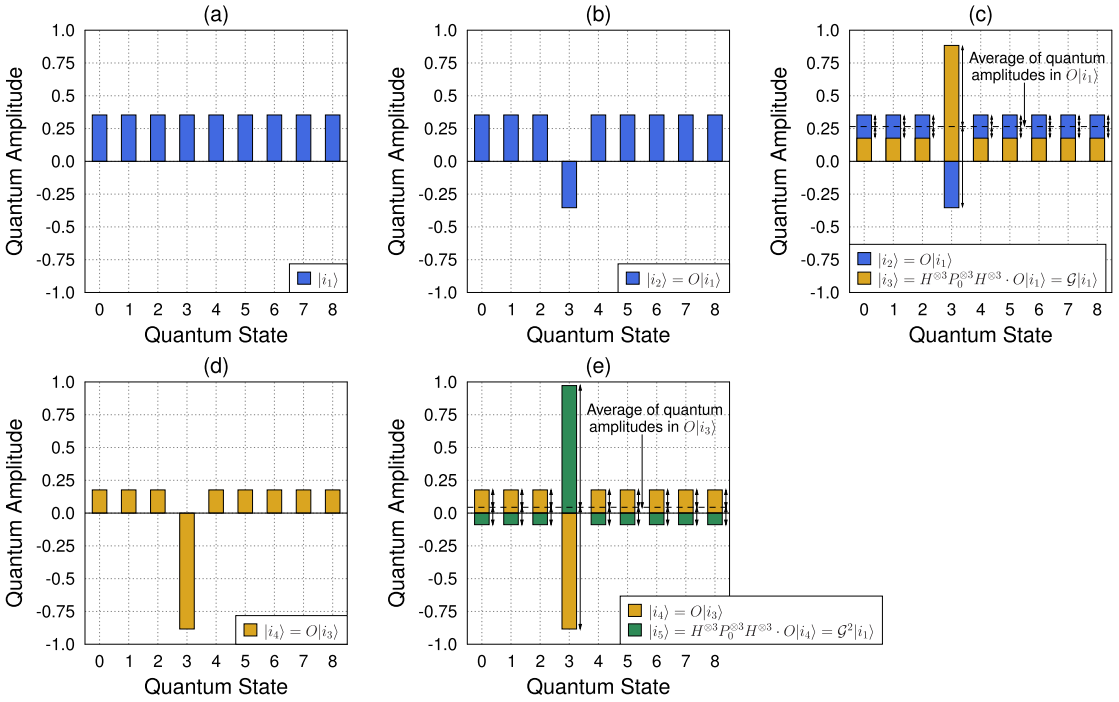

FIGURE 4. The evolution of the quantum amplitudes of Grover's algorithm, when employed in a database with $N = 8$ entries, where the single solution ($S = 1$) lies in the quantum state $|3\rangle = |011\rangle$ A pair of Grover iterations are applied, before observing the resultant quantum register $|i_5\rangle$. (a) Initialization. (b) First Oracle Operation. (c) First Diffusion Operation. (d) Second Oracle Operation. (e) Second Diffusion Operation.

also in the value register $|f(x)\rangle$. After observing the resultant state $\mathcal{G}^{L_{opt}}|\psi_2\rangle$, there is a success probability of

$$P_{success} = \sin^2\left[(2L_{opt}+1)\cdot \arcsin\left(\sqrt{\frac{S}{N}}\right)\right] \quad (32)$$

for obtaining a solution $|x\rangle$. However, Grover's QSA requires prior knowledge of S, which may not always be possible in engineering applications.

Since a universal quantum computer, which would be able to implement Grover's QSA does not exist at the time of writing, the actual complexity of each gate will depend on the specific technology that will be used to design such a machine. Therefore, following the pioneers of QSAs [36], [38], [39], [51], even though U_f may be employed only once in the initialization stage, assuming that strong quantum error correction codes are employed for stabilizing the quantum system [52], let us proceed by stipulating the simplifying assumption that the complexity of a single Grover iteration is equivalent to that of a single CFE performed in the classical domain.

Figure 4 describes an example of Grover's QSA, when used for finding the one and only solution ($S = 1$) in a database having $N = 8$ entries. Since the number of solutions is known prior to the quantum search, the optimal number of times that Grover's operator $\mathcal{G}$ should be applied is $L_{opt} = \left\lfloor \frac{\pi}{4}\sqrt{\frac{N}{S}} \right\rfloor = 2$.

Initially, the system's quantum state is prepared in the superposition of states $|\psi_{1,U_f}\rangle$ as described in (31). At that stage, the index register $|i\rangle$ is entangled with the value register, as encapsulated in

$$\begin{aligned}|\psi_{1,U_f}\rangle &= 0.354\cdot(|000\rangle|f(000)\rangle + |001\rangle|f(001)\rangle \\ &\quad + |010\rangle|f(010)\rangle + |011\rangle|f(011)\rangle \\ &\quad + |100\rangle|f(100)\rangle + |101\rangle|f(101)\rangle \\ &\quad + |110\rangle|f(110)\rangle + |111\rangle|f(111)\rangle) \\ &= 0.3536\cdot(|0\rangle|f(0)\rangle + |1\rangle|f(1)\rangle + |2\rangle|f(2)\rangle \\ &\quad + |3\rangle|f(3)\rangle + |4\rangle|f(4)\rangle + |5\rangle|f(5)\rangle \\ &\quad + |6\rangle|f(6)\rangle + |7\rangle|f(7)\rangle). \end{aligned} \quad (33)$$

In our scenario, we are searching for the specific value δ, which - as it eventually turns out, but is not known to us *a priori* - is only found in $f(3)$. Therefore, $|3\rangle = |011\rangle$ is the desired solution. For simplicity, let us omit the value register from the subsequent steps of Grover's QSA, as well as from Fig. 4, but keeping in mind that it will remain entangled to the corresponding states of the index register throughout Grover's QSA. If quantum noise was applied to the circuit, both the index and the value registers should be jointly analysed and quantum error correction codes should be employed. Since in this contribution we assume noiseless and error-free quantum operations, we may proceed by investigating only the index register, which may be described as

$$\begin{aligned}|i_1\rangle &= 0.354\cdot(|0\rangle + |1\rangle + |2\rangle + |3\rangle \\ &\quad + |4\rangle + |5\rangle + |6\rangle + |7\rangle). \end{aligned} \quad (34)$$

Figure 4a shows the initial equiprobable superposition of the $N = 8$ states. When the Oracle operator is applied during

the first Grover iteration, the sign of the solution index $|3\rangle$ is flipped, as presented in Fig. 4b and encapsulated in

$$|i_2\rangle = O|i_1\rangle = 0.3536 \cdot (|0\rangle + |1\rangle + |2\rangle - |3\rangle + |4\rangle + |5\rangle + |6\rangle + |7\rangle). \quad (35)$$

The diffusion operator $D = HP_0H$ is then applied to $|i_2\rangle$, resulting in a reflection of all the superimposed states with respect to their average quantum amplitude, which is equal to $\mu_{i_2} = (0.354 \cdot 7 - 0.354)/8 = 0.266$, as it is graphically captured in Fig. 4c. The amplitude of the solution index is reflected from -0.3536 to $2 \cdot \mu_{i_2} - (-0.354) = 0.885$, while the amplitudes of the rest of the states are evolved from 0.354 to $2 \cdot \mu_{i_2} - (0.354) = 0.179$, resulting in

$$\begin{aligned} |i_3\rangle &= HP_0H \cdot O|i_2\rangle = \mathcal{G}|i_1\rangle \\ &= 0.179 \cdot |0\rangle + 0.179 \cdot |1\rangle + 0.179 \cdot |2\rangle + 0.885 \cdot |3\rangle \\ &\quad + 0.179 \cdot |4\rangle + 0.179 \cdot |5\rangle + 0.179 \cdot |6\rangle + 0.179 \cdot |7\rangle. \end{aligned} \quad (36)$$

Observing the index register at this point would yield a probability of success equal to the probability of observing the state $|3\rangle$, which is $0.885^2 = 0.783$, or 78.3%. Since the optimal number of Grover iterations was calculated to be equal to $L_{opt} = 2$, we can expect for the probability of success to be even higher after another application of Grover's operator. Indeed, by applying the Oracle operator for a second time, followed by the diffusion operator yields

$$\begin{aligned} |i_4\rangle &= O|i_3\rangle \\ &= 0.179 \cdot |0\rangle + 0.179 \cdot |1\rangle + 0.179 \cdot |2\rangle - 0.885 \cdot |3\rangle \\ &\quad + 0.179 \cdot |4\rangle + 0.179 \cdot |5\rangle + 0.179 \cdot |6\rangle + 0.179 \cdot |7\rangle \end{aligned} \quad (37)$$

and

$$\begin{aligned} |i_5\rangle &= HP_0H \cdot O|i_4\rangle = \mathcal{G}|i_3\rangle = \mathcal{G}^2|i_1\rangle \\ &= -0.087 \cdot |0\rangle - 0.087 \cdot |1\rangle - 0.087 \cdot |2\rangle + 0.977 \cdot |3\rangle \\ &\quad - 0.087 \cdot |4\rangle - 0.087 \cdot |5\rangle - 0.087 \cdot |6\rangle - 0.087 \cdot |7\rangle, \end{aligned} \quad (38)$$

as illustrated in Fig. 4d and Fig. 4e, respectively. In (38), the average value $\mu_{i_4} = (0.179 \cdot 7 - 0.885)/8 = 0.046$ of the quantum amplitudes of $|i_4\rangle$ was used for evolving the amplitude of the solution state from -0.885 to $2\mu_{i_4} - (-0.885) = 0.977$ and those of the non-solution states from 0.179 to $2\mu_{i_4} - 0.179 = -0.087$.

Therefore, if the quantum index register was observed in the state $|i_5\rangle$, the success probability would be equal to $0.977^2 = 0.955$ or 95.5%. When Grover's QSA is employed in databases having a higher size N, the success probability approaches 100%, but more Grover iterations are required to achieve that.

B. BOYER-BRASSARD-HØYER-TAPP QSA

Boyer *et al.* in [38] proposed a variant of Grover's QSA, removing the requirement of having prior knowledge of S. The only difference with respect to Grover's QSA of Section III-A is that since the optimal number of times that the Grover operator should be applied is now unknown, it is applied a pseudorandom number of times, following a specific methodology that guarantees $\sim 100\%$ success probability before reaching $4.5\sqrt{N}$ number of Grover iterations.

C. DÜRR-HØYER ALGORITHM

Dürr and Høyer [39] presented another variant of Grover's QSA, which also relies on the variant proposed by Boyer *et al.* in [38]. The so-called DHA succeeds in finding the specific index that corresponds to the minimum value of the function after $O(\sqrt{N})$ with $\sim 100\%$ success probability. Starting from a randomly chosen index, we set δ equal to that index's CF value. Then, the BBHT QSA is invoked for finding an index that has a CF value lower than δ. This may be readily implemented by using a quantum bit string comparator circuit in the Oracle that may output whether a value is greater than, smaller than, or equal to δ, as described in [50]. Once such an index has been found, its CF value becomes the new δ and the same process is repeated until no index with a CF value smaller than the last updated δ is found. In [8] we showed that a complexity reduction may be achieved if a carefully picked CF value is used for initializing δ, instead of choosing a random index's CF value.

IV. QUANTUM-ASSISTED PARTICLE SWARM OPTIMIZATION

The PSO employs Z number of particles over Ξ generations. In our application, a particle's position is represented by the discrete-valued perturbation vector $\mathbf{w}$ of (1) in the discrete-valued QPSO and by the continuous-valued signal vector in the continuous-valued QPSO. Both are appraised with respect to the CF value associated with it, where the CF is the error probability of (28). During the ξth generation of the dQPSO, $\xi \in \{1, 2, \ldots, \Xi\}$, the ζth particle, $\zeta \in \{1, 2, \ldots, Z\}$ has a U-element position $\mathbf{w}_\zeta^{(\xi)} = \left[w_{\zeta,1}^{(\xi)}, \ldots, w_{\zeta,U}^{(\xi)}\right]^T$ and a U-element velocity $\mathbf{v}_\zeta^{(\xi)} = \left[\mathrm{v}_{\zeta,1}^{(\xi)}, \mathrm{v}_{\zeta,1}^{(\xi)}, \ldots, \mathrm{v}_{\zeta,U}^{(\xi)}\right]^T$. Similarly, during the ξth generation of the cQPSO, $\xi \in \{1, 2, \ldots, \Xi\}$, the ζth particle, $\zeta \in \{1, 2, \ldots, Z\}$ has an N_T-element position $\mathbf{d}_\zeta^{(\xi)} = \left[d_{\zeta,1}^{(\xi)}, d_{\zeta,1}^{(\xi)}, \ldots, d_{\zeta,N_T}^{(\xi)}\right]^T$ and an N_T-element velocity $\mathbf{v}_\zeta^{(\xi)} = \left[\mathrm{v}_{\zeta,1}^{(\xi)}, \mathrm{v}_{\zeta,1}^{(\xi)}, \ldots, \mathrm{v}_{\zeta,N_T}^{(\xi)}\right]^T$. Throughout the generations, each particle adjusts its personal position and velocity, based on its own "best so-far" position, as well as on the best so-far global position, up to that generation. It may be considered as the operation of a society with a common goal, where each individual adjusts its behaviour relying on its own experience, as well as on that of the community.

In this contribution, we propose a pair of QPSO algorithms by employing the DHA for performing quantum search in the population of each generation of both the discrete-valued and of the continuous-valued PSO algorithms. It should be noted that in contrast to Grover's QSA, both the BBHT QSA and

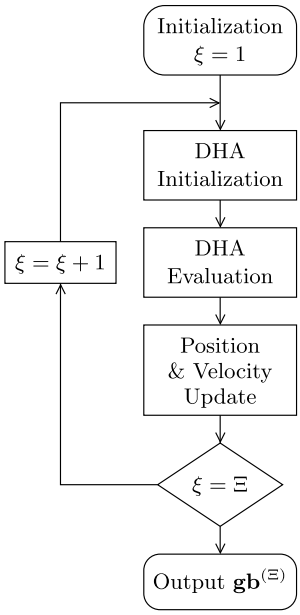

FIGURE 5. Flow chart of the QPSO, describing the operation of both the dQPSO and the cQPSO.

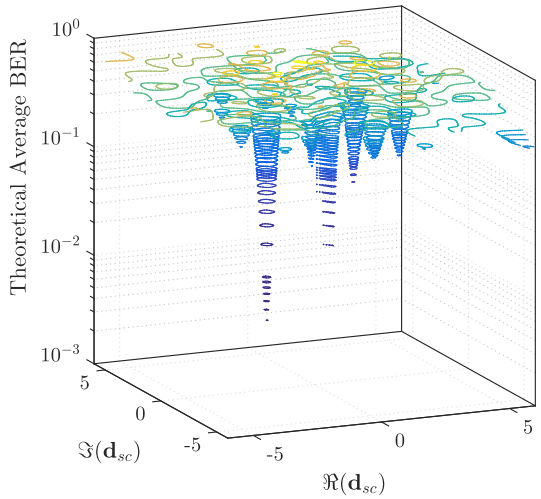

FIGURE 6. Three-dimensional contour plot of the theoretical average MBER calculated by (28) with respect to the signal vector for the specific scenario of Section IV.

the DHA constitute trial-and-error based algorithms, since the optimal number of Grover iterations L_{opt} is unknown. Therefore, a number K of the N legitimate indices x and their corresponding CF values $f(x)$ will become available in the classical domain, including the solution to the search problem, for $K < N$. We may exploit this fact, by using the DHA for finding the "better", or more "suitable", particles in every generation of the PSO and allow them to survive and be updated for the subsequent generations. When compared to the classical PSO, the QPSO may require a lower number of CFEs for achieving an equivalent performance, when the population size of these two algorithms is the same, or yield an improved BER performance associated with the same computational complexity, when a higher population size is searched through during each generation of the QPSO. The flow chart of the QPSO is presented in Fig. 5, which describes the operation of both the dQPSO and the cQPSO.

For ease of presentation, let us proceed by portraying the proposed dQPSO algorithm, while applying it to a rank-deficient multi-carrier and multi-user scenario, where a BS having $N_T = 1$ transmit AE supports $U = 2$ users by transmitting QPSK symbols with the aid of $Q = 1024$ subcarriers. The normalized user load is $U_L = U/N_T = 2$, the $(U \times N_T) = (2 \times 1)$-element FD-CHTF $\mathbf{H}_{sc}$ at the first subcarrier is

$$\mathbf{H}_{sc} = \begin{bmatrix} -1.47 + j \cdot 0.81 \\ 0.82 - j \cdot 0.96 \end{bmatrix}, \tag{39}$$

while the symbol vector $\mathbf{x}_{sc}$ of the scenario, that has to be conveyed to the users is

$$\mathbf{x}_{sc} = \begin{bmatrix} -0.71 + j \cdot 0.71 \\ -0.71 - j \cdot 0.71 \end{bmatrix}. \tag{40}$$

Assuming that the system is operating at an average SNR of 15 dB, which corresponds to $\sigma_n^2 = 0.032$, the precoding matrix is calculated based on (2) as

$$\begin{aligned} \mathbf{P}_{sc} &= \mathbf{H}_{sc}^H \left(\mathbf{H}_{sc} \mathbf{H}_{sc}^H + \sigma_n^2 \mathbf{I}_U \right)^{-1} \\ &= [-0.33 - j \cdot 0.18, \quad 0.18 + j \cdot 0.21]. \end{aligned} \tag{41}$$

Therefore the signal vector without vector perturbation would be equal to

$$\mathbf{d}_{sc,\mathbf{w}=\{0\}^U} = \mathbf{P}_{sc} \cdot \mathbf{x}_{sc} = [0.38 - j \cdot 0.39]. \tag{42}$$

The proposed quantum-assisted dPSO aims for finding the specific perturbation vector $\mathbf{w}$, and therefore $\mathbf{d}_{sc}$ that would minimize the BER criterion of (28). Figure 6 shows the theoretical average BER of (28) calculated for a range of $\mathbf{d}_{sc} = [-6, 6] + j[-6, 6]$. We may observe the multiple local minima that occur, since our scenario is rank-deficient. The optimal $N_T = 1$-element signal vector $\mathbf{d}_{sc}$ seems to be close to $\mathbf{d}_{sc} = [-1.68 + j \cdot 0.55]$. This is more visible in the two-dimensional contour plot of the theoretical average BER of (28), which is plotted in Fig. 7a, along with the associated colorbar. Based on Fig. 7a we should also note the apparent symmetry of the theoretical average BER with respect to $[0 + j \cdot 0]$, due to the fact that when a signal vector $\mathbf{d}_{sc}$ is expected to yield a low BER, the exact opposite signal vector $\mathbf{d}'_{sc} = -\mathbf{d}_{sc}$ will be expected to result in a degraded performance according to (28). Let us now proceed to the analysis of the dQPSO, while applying it to our scenario with the aid of $Z_d = 64$ particles and $\Xi_d = 2$ generations.

A. DISCRETE-VALUED QPSO

The dQPSO is invoked after the MMSE-based calculation of the precoding matrix $\mathbf{P}$.

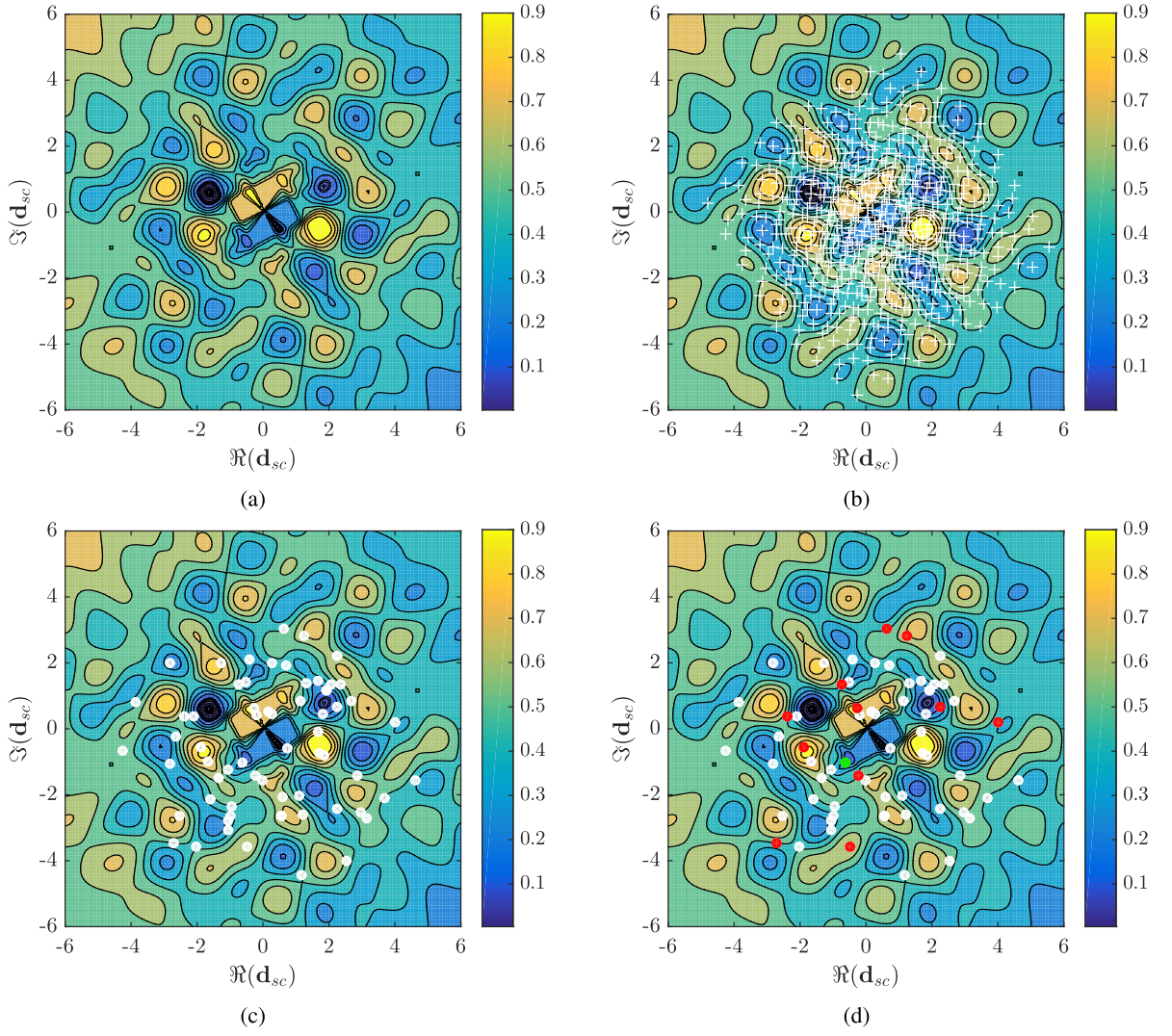

FIGURE 7. Two-dimensional contour plot of the theoretical average BER calculated by (28) with respect to the signal vector $\mathbf{d}_{sc}$ for the specific scenario of Section IV, along with positions of the particles during the first generation of the dQPSO. (a) The global minimum BER is in the area around $\mathbf{d}_{sc} = [-1.68 + j \cdot 0.55]$. (b) The full search space of the discrete perturbation vector search, represented by the resultant signal vectors (white crosses), when the 625 legitimate perturbation vectors are employed, as described in (44). (c) The positions of the $Z_d = 64$ particles during the first generation of the dQPSO (white dots). (d) The positions of the $Z_d = 64$ particles during the first generation of the dQPSO (white dots), as well as the positions of the $K_{d,1} = 12$ particles that were observed by the DHA (red dots) after $A_d = 15$ CFEs during the first generation. The best evaluated particle (green dot) is the second best particle of the generation.

1) INITIALIZATION

The position of the ζth particle during the first generation $\mathbf{w}_\zeta^{(1)}$ is randomly initialized in the search space

$$W = \{-2, -1, 0, 1, 2\}^{\otimes U} + j \cdot \{-2, -1, 0, 1, 2\}^{\otimes U}. \quad (43)$$

Again, as mentioned in Section II, the search space W has been obtained via extensive simulations of different scenarios, where we tracked the minimum and maximum values of the optimal discrete perturbation vector with respect to the MBER criterion. We have found that the set $\{-2, -1, 0, 1, 2\}$ for both the real and imaginary part of each user's perturbation includes ∼100% of the optimal discrete perturbation vectors. Therefore, the resultant signal vector $\mathbf{d}$ lies in the search space D, where D is

$$D = \mathbf{P}\left(\mathbf{x} + \begin{bmatrix} \{-2, -1, 0, 1, 2\} + j\{-2, -1, 0, 1, 2\} \\ \vdots \\ \{-2, -1, 0, 1, 2\} + j\{-2, -1, 0, 1, 2\} \end{bmatrix}\right). \quad (44)$$

The velocity of each particle is initially set to 0. More precisely, the position of a particle in the dQPSO represents a legitimate complex perturbation selected for each user's symbol within the set $\{-2, -1, 0, 1, 2\} + j\{-2, -1, 0, 1, 2\}$. Note that even though $\mathbf{d}_\zeta^{(\xi)}$ is used as the position of a particle during the evaluation stage, the discrete-valued position will be described by its associated discrete-valued

perturbation vector $\mathbf{w}_{\zeta}^{(\xi)}$, as encapsulated in the search space of (44).

In our scenario, the full search space is illustrated in Fig. 7b, while the positions of the $Z_d = 64$ number of particles during the first generation, randomly created in the search space D of (44) are presented in Fig. 7c. Since we have opted for $Z_d = 64$ particles, $\log_2(Z_d) = 6$ qubits are required for creating the population of the first generation. The number of required qubits only depends on the desired population size during each generation. The higher the population size is, the higher the probability of a better particle appearing in the population becomes. However, at the same time, more qubits are required for representing the population in the quantum domain and a higher complexity has to be invoked for searching in a higher search space.

2) DHA-BASED EVALUATION

Even though in the classical PSO the positions of all Z_d particles would be evaluated during each generation based on the CF value of (28), hence resulting in Z_d CFEs, in the proposed QPSO the DHA is employed for searching for the specific particle having the position that corresponds to the minimum CF value of (28) in the ξth generation. Since the DHA is a probabilistic algorithm exhibiting a variable complexity, we opt for stopping the operation of the DHA after a predetermined number of A_d Grover iterations, or, equivalently, CFEs.

The complexity of the proposed QPSO does not depend on the population size Z_d, but rather on the adjustable number of Grover iterations allowed before the termination of the DHA. Therefore, a higher population size Z_d would increase the pool size and hence improves the performance, but it would also require more particle position and velocity updates during each generation. It should be noted that choosing a low number A_d may result in stopping the search algorithm before finding the best particle, while selecting a high A_d may result in requiring unnecessary extra complexity. As discussed in Section IV, after the DHA's operation we will have obtained $K_{d,\xi}$ particles' CF values in the classical domain, with $K_{d,\xi}$ having a different value during each generation, due to the probabilistic nature of the DHA.

In our scenario, after $A_d = 15$ CFEs, the DHA observed $K_{d,1} = 12$ particles, which are represented by a red dot in Fig. 7d. Therefore, the positions and CF values of only those $K_{d,1} = 12$ particles are available. The position of the best evaluated particle, shown as a green dot in Fig. 7d, is the $\zeta = 10$th particle of the generation, which is associated with the discrete-valued perturbation vector $\mathbf{w}_{sc,\,best} = [2 + j \cdot 2,\ 2 + j \cdot 2]^T$, resulting in the distance vector $\mathbf{d}_{sc,\,best} = [-0.62 - j \cdot 1.04]$ and a theoretical average BER of 0.19. We should note that this is actually the second best particle of the generation. This means that if we had allowed more CFEs in the DHA, associated with a higher A_d, the best particle of the generation would have been observed. Nevertheless, as seen in Fig. 7c, none of the particles in the first generation has a position in the area of the global minimum.

3) POSITION & VELOCITY UPDATE

After the evaluation step during the ξth generation, the personal best position of the ζth particle $\mathbf{pb}_{\zeta}^{(\xi)} = \left[pb_{\zeta,1}^{(\xi)}, \ldots, pb_{\zeta,U}^{(\xi)}\right]^T$ is updated, but only if that particle was one of the $K_{d,\xi}$ particles, which were observed by the DHA, according to

$$\mathbf{pb}_{\zeta}^{(\xi)} = \begin{cases} \mathbf{w}_{\zeta}^{(\xi)} & \text{if } P_e\left(\mathbf{d}_{\zeta}^{(\xi)}\right) < P_e\left(\mathbf{d}_{\zeta,pb}^{(\xi-1)}\right) \\ \mathbf{pb}_{\zeta}^{(\xi-1)} & \text{if } P_e\left(\mathbf{d}_{\zeta}^{(\xi)}\right) \geq P_e\left(\mathbf{d}_{\zeta,pb}^{(\xi-1)}\right), \end{cases} \tag{45}$$

where $\mathbf{d}_{\zeta}^{(\xi)} = \mathbf{P} \cdot \left(\mathbf{x} + \mathbf{w}_{\zeta}^{(\xi)}\right)$ and $\mathbf{d}_{\zeta,pb}^{(\xi-1)} = \mathbf{P} \cdot \left(\mathbf{x} + \mathbf{pb}_{\zeta}^{(\xi-1)}\right)$.

In our scenario, only the specific $K_{d,1} = 12$ particles' positions will be updated during the first generation, while the personal best position of the rest will remain unavailable. For example, the personal best position of the best evaluated particle, associated with $\mathbf{w}_{sc,\,best} = [2 + j \cdot 2,\ 2 + j \cdot 2]^T$, which is the $\zeta = 10$th particle of the generation, is updated as in

$$\mathbf{pb}_{10}^{(1)} = \mathbf{w}_{10}^{(1)} = \begin{bmatrix} 2 + j \cdot 2 \\ 2 + j \cdot 2 \end{bmatrix}. \tag{46}$$

The rest of the evaluated particles are similarly updated.

Then, the global best position of the ξth generation $\mathbf{gb}^{(\xi)} = \left[gb_1^{(\xi)}, \ldots, gb_U^{(\xi)}\right]^T$ is calculated based on

$$\mathbf{gb}^{(\xi)} = \begin{cases} \mathbf{pb}_{\zeta_{best}}^{(\xi)} & \text{if } P_e\left(\mathbf{d}_{\zeta_{best},pb}^{(\xi)}\right) < P_e\left(\mathbf{d}_{gb}^{(\xi-1)}\right) \\ \mathbf{gb}^{(\xi-1)} & \text{if } P_e\left(\mathbf{d}_{\zeta_{best},pb}^{(\xi)}\right) \geq P_e\left(\mathbf{d}_{gb}^{(\xi-1)}\right), \end{cases} \tag{47}$$

where $\mathbf{pb}_{\zeta_{best}}^{(\xi)}$ is the personal best position of the best particle of the ξth generation, $\mathbf{d}_{\zeta_{best},pb}^{(\xi)} = \mathbf{P} \cdot \left(\mathbf{x} + \mathbf{pb}_{\zeta_{best}}^{(\xi)}\right)$ and $\mathbf{d}_{gb}^{(\xi-1)} = \mathbf{P} \cdot \left(\mathbf{x} + \mathbf{gb}^{(\xi-1)}\right)$.

In our scenario, the global best position of the $\xi = 1$st generation is updated as in

$$\mathbf{gb}^{(1)} = \mathbf{pb}_{10}^{(1)} = \begin{bmatrix} 2 + j \cdot 2 \\ 2 + j \cdot 2 \end{bmatrix}, \tag{48}$$

since the $\zeta_{best} = 10$th particle is the best particle of the first generation.

Having updated the particles' personal best position, as well as the global best position, we may update the velocity of each particle in a different way from that of the classical PSO, depending on whether that particle was measured during the ξth generation by the DHA, or not. More specifically, if the ζth particle during the ξth generation was observed by the DHA, then the velocity of its uth dimension, which is associated with $\mathbf{v}_{\zeta}^{(\xi)} = \left[\mathrm{v}_{\zeta,1}^{(\xi)}, \ldots, \mathrm{v}_{\zeta,U}^{(\xi)}\right]^T$ and $u \in \{1, 2, \ldots, U\}$, is updated similarly to the PSO according to

$$\begin{aligned} \mathrm{v}_{\zeta,u}^{(\xi)} = {} & g \cdot \mathrm{v}_{\zeta,u}^{(\xi-1)} + u_1 \cdot c_1 \cdot \Re\left\{pb_{\zeta,u}^{(\xi)} - w_{\zeta,u}^{(\xi)}\right\} \\ & + j \cdot u_2 \cdot c_2 \cdot \Im\left\{pb_{\zeta,u}^{(\xi)} - w_{\zeta,u}^{(\xi)}\right\} \\ & + u_3 \cdot c_1 \cdot \Re\left\{gb_u^{(\xi)} - w_{\zeta,u}^{(\xi)}\right\} \\ & + j \cdot u_4 \cdot c_2 \cdot \Im\left\{gb_u^{(\xi)} - w_{\zeta,u}^{(\xi)}\right\}, \end{aligned} \tag{49}$$

where $u_1, u_2, u_3, u_4 \in \mathcal{U}(0,1)$ are numbers randomly generated from the uniform distribution, while $c_1 = c_2 = 0.5$ were found to provide a good performance based on our empirical simulations, where many values were selected for c_1 and c_2. The generation-based inertia weight g is calculated as [53]

$$g = g_{\min} + (g_{\max} - g_{\min}) \cdot \frac{\Xi - \xi}{\Xi}, \tag{50}$$

with $g_{\min} = 0.4$ and $g_{\max} = 0.9$. If the ζth particle's CF value during the ξth generation was not obtained during the DHA's operation, the velocity of its uth dimension, for $u \in \{1, 2, \ldots, U\}$ is updated relying only on its $(\xi - 1)$st generation's velocity and on the global best position of the current ξth generation, as encapsulated in

$$\begin{aligned} \mathrm{v}_{\zeta,u}^{(\xi)} = {} & g \cdot \mathrm{v}_{\zeta,u}^{(\xi-1)} + u_3 \cdot c_2 \cdot \Re\left\{ gb_u^{(\xi)} - w_{\zeta,u}^{(\xi)} \right\} \\ & + j \cdot u_4 \cdot c_2 \cdot \Im\left\{ gb_u^{(\xi)} - w_{\zeta,u}^{(\xi)} \right\}. \end{aligned} \tag{51}$$

The reasoning behind updating the velocity of a particle, which was not observed, without relying on its personal best position is that - with a high probability - this particle was not picked by the DHA, because its personal position was not good enough. Therefore, we opted for "moving" it towards the neighbourhood of the global best solution of the ξth generation, where it may have a position corresponding to a lower error probability. In Section V we compare different choices for the update of the particles' velocities, with respect to the resultant BER performance.

In our scenario, the velocity of all $Z_d = 64$ particles will be updated. During the $\xi = 1$st generation, the velocities of the $K_{d,1} = 12$ observed particles will be updated according to (49), while the remaining $Z_d - K_{d,1} = 52$ particles' velocities will be updated according to (51). Since we are considering the $\xi = 1$st generation and there will be a total of $\Xi = 2$ generations, according to (50) we have $g = 0.65$. Let us describe the velocity update of the $\zeta = 50$th particle, which was observed by the DHA, and the $\zeta = 2$nd particle, which was not. Since the $\zeta = 50$th particle was observed and we have $U = 2$ users, its velocity $\mathrm{v}_{50}^{(1)} = [\mathrm{v}_{50,1}^{(1)}, \mathrm{v}_{50,2}^{(1)}]^T$ will be updated based on (49) and it would result in

$$\begin{aligned} \mathrm{v}_{50,1}^{(1)} = {} & 0.65 \cdot (0 + j \cdot 0) + 0.88 \cdot 0.5 \cdot (1 - 1) \\ & + j \cdot 0.44 \cdot 0.5 \cdot (1 - 1) \\ & + 0.44 \cdot 0.5 \cdot (2 - 1) \\ & + j \cdot 0.80 \cdot 0.5 \cdot (2 - 1) \\ = {} & 0.17 + j \cdot 0.40 \end{aligned} \tag{52}$$

$$\begin{aligned} \mathrm{v}_{50,2}^{(1)} = {} & 0.65 \cdot (0 + j \cdot 0) + 0.81 \cdot 0.5 \cdot (-2 + 2) \\ & + j \cdot 0.58 \cdot 0.5 \cdot (-1 + 1) \\ & + 0.22 \cdot 0.5 \cdot (2 + 2) \\ & + j \cdot 0.13 \cdot 0.5 \cdot (2 + 1) \\ = {} & 0.44 + j \cdot 0.19. \end{aligned} \tag{53}$$

On the other hand, since the $\zeta = 2$nd particle was not observed during the first generation, its velocity $\mathrm{v}_2^{(1)} = [\mathrm{v}_{2,1}^{(1)}, \mathrm{v}_{2,2}^{(1)}]^T$ will be updated according to (51), as encapsulated in

$$\begin{aligned} \mathrm{v}_{2,1}^{(1)} = {} & 0.65 \cdot (0 + j \cdot 0) + 0.58 \cdot 0.5 \cdot (2 - 1) \\ & + j \cdot 0.19 \cdot 0.5 \cdot (2 - 0) \\ = {} & 0.29 + j \cdot 0.19 \end{aligned} \tag{54}$$

$$\begin{aligned} \mathrm{v}_{2,2}^{(1)} = {} & 0.65 \cdot (0 + j \cdot 0) + 0.64 \cdot 0.5 \cdot (2 + 2) \\ & + j \cdot 0.64 \cdot 0.5 \cdot (2 - 2) \\ = {} & 1.28 + j \cdot 0. \end{aligned} \tag{55}$$

In order to update the discrete-valued position of the ζth particle during the ξth generation, we first convert its associated velocity to the $[0, M-1]$ interval by using the sigmoid function advocated in [54]

$$\begin{aligned} sig\left(\Re\left\{\mathbf{v}_\zeta^{(\xi)}\right\}\right) &= \frac{M-1}{1 + e^{-\Re\left\{\mathrm{v}_\zeta^{(\xi)}\right\}}}, \\ sig\left(\Im\left\{\mathbf{v}_\zeta^{(\xi)}\right\}\right) &= \frac{M-1}{1 + e^{-\Im\left\{\mathrm{v}_\zeta^{(\xi)}\right\}}}, \end{aligned} \tag{56}$$

where $M = 5$ is the range of the single-dimensional discrete search space $\{-2, 1, 0, 1, 2\}$. The uth dimension of the ζth particle's position during the ξth generation is updated according to

$$\begin{aligned} w_{\zeta,u}^{(\xi)} = {} & \left\lfloor sig\left(\Re\left\{\mathrm{v}_{\zeta,u}^{(\xi)}\right\}\right) + (M-1) \cdot \rho \cdot r_1 \right\rceil \\ & + j \cdot \left\lfloor sig\left(\Im\left\{\mathrm{v}_{\zeta,u}^{(\xi)}\right\}\right) + (M-1) \cdot \rho \cdot r_2 \right\rceil, \end{aligned} \tag{57}$$

where the choice of $\rho = 0.1$ offers a good performance and $r_1, r_2 \in \mathcal{N}(0,1)$ are randomly generated numbers from the zero-mean and unit-variance normal distribution. Therefore, all particles' positions are updated following the same rule, regardless of whether they were observed during the ξth generation by the DHA. In order to guarantee that the position of a particle is in the search range of (44), after (57) we apply

$$\begin{aligned} \Re\left\{w_{\zeta,u}^{(\xi)}\right\} &= \begin{cases} -\dfrac{M-1}{2}, & \Re\left\{w_{\zeta,u}^{(\xi)}\right\} < -\dfrac{M-1}{2} \\ \Re\left\{w_{\zeta,u}^{(\xi)}\right\}, & -\dfrac{M-1}{2} \le \Re\left\{w_{\zeta,u}^{(\xi)}\right\} \le \dfrac{M-1}{2} \\ \dfrac{M-1}{2}, & \Re\left\{w_{\zeta,u}^{(\xi)}\right\} > \dfrac{M-1}{2} \end{cases} \\ \Im\left\{w_{\zeta,u}^{(\xi)}\right\} &= \begin{cases} -\dfrac{M-1}{2}, & \Im\left\{w_{\zeta,u}^{(\xi)}\right\} < -\dfrac{M-1}{2} \\ \Im\left\{w_{\zeta,u}^{(\xi)}\right\}, & -\dfrac{M-1}{2} \le \Im\left\{w_{\zeta,u}^{(\xi)}\right\} \le \dfrac{M-1}{2} \\ \dfrac{M-1}{2}, & \Im\left\{w_{\zeta,u}^{(\xi)}\right\} > \dfrac{M-1}{2}. \end{cases} \end{aligned} \tag{58}$$

In our scenario, all particles' position will be updated according to (56), (57) and (58). Let us describe the update of the $\zeta = 50$th particle's position. Initially, we convert its

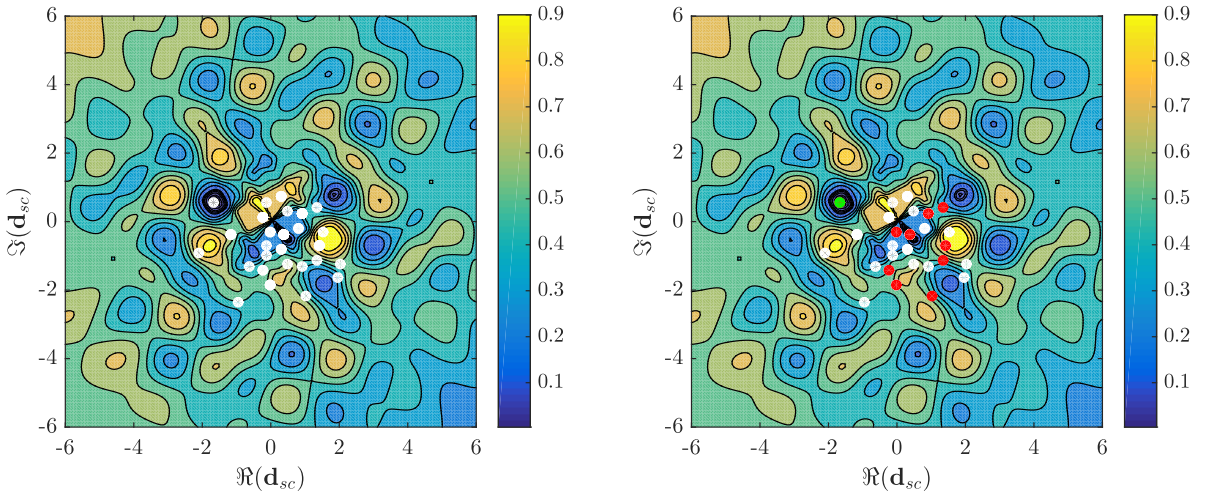

FIGURE 8. Two-dimensional contour plot of the theoretical average BER calculated by (28) with respect to the signal vector $\mathbf{d_{sc}}$ for the specific scenario of Section IV, along with positions of the particles during the second generation of the dQPSO. (a) The positions of the $Z_d = 64$ particles during the second generation of the dQPSO (white dots). (b) The positions of the $Z_d = 64$ particles during the second generation of the dQPSO (white dots), as well as the positions of the $K_{d,2} = 11$ particles that were observed by the DHA (red dots) after $A_d = 15$ CFEs during the second generation. The best evaluated particle (green dot) is the global best particle of the discrete optimization problem.

velocity by using the sigmoid function of (56), resulting in

$$sig\left(\Re\left\{\mathbf{v}_{50}^{(1)}\right\}\right) = \frac{4}{1+e^{-\Re\left\{\mathbf{v}_{50}^{(1)}\right\}}} = \begin{bmatrix}2.17\\2.42\end{bmatrix},$$
$$sig\left(\Im\left\{\mathbf{v}_{50}^{(1)}\right\}\right) = \frac{4}{1+e^{-\Im\left\{\mathbf{v}_{50}^{(1)}\right\}}} = \begin{bmatrix}2.39\\2.19\end{bmatrix}. \quad (59)$$

Finally, according to (57), the updated position of the $\zeta = 50$th particle in the $\xi = 1$st generation is

$$\begin{aligned} w_{50,1}^{(1)} &= \lfloor 2.17 + 4 \cdot 0.1 \cdot (-0.39) \rceil \\ &\quad + j \cdot \lfloor 2.39 + 4 \cdot 0.1 \cdot (-0.33) \rceil, \\ &= 2 + j \cdot 2, \end{aligned} \quad (60)$$

$$\begin{aligned} w_{50,2}^{(1)} &= \lfloor 2.42 + 4 \cdot 0.1 \cdot (-1.39) \rceil \\ &\quad + j \cdot \lfloor 2.19 + 4 \cdot 0.1 \cdot 0.31 \rceil, \\ &= 2 + j \cdot 2. \end{aligned} \quad (61)$$

4) DHA INITIALIZATION

During the ξth generation, the initial δ for the DHA's search is chosen to be the best particle's CF value from the $(\xi-1)$st generation, but only if that particle is also the global best particle up to the ξth generation. Otherwise, the DHA is randomly initialized with the CF value of a random particle's position. This methodology succeeds in reducing the complexity required for finding the best particle of the generation, when a worthy particle is present, while allowing a wider search, when the evolution is inaccurately navigated. During the first generation, the DHA is randomly initialized.

Naturally, there is a particle during the first generation that has the globally best position, therefore δ for the DHA's search in the $\xi = 2$nd generation is initialized to that particle's CF value. In our scenario, this corresponds to the CF value of the $\zeta = 10$th particle, which is equal to $\delta = 0.19$. During the $\xi = 2$nd generation, all $Z_d = 64$ particles' positions are depicted in Fig. 8a. The specific particles of the second generation that were observed by the DHA are plotted in Fig. 8b, along with the best found particle, associated with $\mathbf{w}_{sc,\,best} = [1 - j \cdot 1,\ 0 + j \cdot 1]^T$ and linked to $\mathbf{d}_{sc,\,best} = [-1.68 + j \cdot 0.55]$.

5) TERMINATION

After a predetermined number of generations Ξ_d, the QPSO is terminated and we conclude that $\mathbf{d}_{opt,discrete} = \mathbf{P}_{sc} \cdot \left(\mathbf{x}_{sc} + \mathbf{gb}^{(\Xi_d)}\right)$.

In our scenario, since $\Xi_d = 2$, only the globally best value is updated after the DHA search in the second generation. Finally, the dQPSO stops and outputs $\mathbf{d}_{opt,discrete} = \mathbf{P}_{sc} \cdot \left(\mathbf{x}_{sc} + \mathbf{gb}^{(\Xi_d)}\right) = [-1.67 + 0.55]$, which is associated with a theoretical average BER value of 0.0033. The dQPSO arrived at the MBER-optimal discrete-valued perturbation vector after $A_d \cdot \Xi_d = 30$ CFEs. At the same time, employing the classical dPSO associated with $Z_d = 6$ and $\Xi_d = 6$ in the same scenario outputs the suboptimal perturbation vector $\mathbf{w}_{sc,PSO} = [0 + j \cdot 0,\ 0 + j \cdot 0]^T$ after $Z_d \cdot \Xi_d = 36$ CFEs, which is associated with the higher theoretical average BER value of 0.054.

B. CONTINUOUS-VALUED QPSO

The cQPSO aims for further improving the output of the dQPSO $\mathbf{d}_{opt,discrete}$, by searching in selected areas, where the discrete optimization could not reach.

1) INITIALIZATION

The cQPSO starts from the point, where the dQPSO ended, by using its output $\mathbf{d}_{opt,discrete}$ in its initial population as the first particle's position $\mathbf{d}_{\zeta}^{(\xi)} = \mathbf{d}_{opt,discrete}$. The remaining $(Z_c - 1)$ particles' positions are randomly generated in the search space $\mathcal{S}^{N_T}$, where

$$\mathcal{S} = [-S_{\max}, S_{\max}] + j \cdot [-S_{\max}, S_{\max}]. \tag{62}$$

The search range depends on the specific nature of the optimization problem, therefore relying on our empirical results, we opt for $S_{\max} = 2$. Please note that in the cQPSO the position of the particle is the continuous-valued signal vector $\mathbf{d}_{\zeta}^{(\xi)}$ and not the discrete-valued perturbation vector $\mathbf{w}_{\zeta}^{(\xi)}$ as in the dQPSO. Hence the position and the velocity of each particle becomes N_T-dimensional in the cQPSO, as opposed to the U-dimensional vectors of the dQPSO.

2) DHA-BASED EVALUATION

The evaluation stage of the cQPSO is the same as that of the dQPSO described in Section IV-A.2, with Z_c number of particles and a predetermined A_c number of Grover iterations during each generation.

3) POSITION & VELOCITY UPDATE

The personal best positions of each particle $\mathbf{pb}_{\zeta}^{(\xi)}$, as well as the global best position $\mathbf{gb}^{(\xi)}$ of the ξth generation in the cQPSO are updated by using the rules of

$$\mathbf{pb}_{\zeta}^{(\xi)} = \begin{cases} \mathbf{d}_{\zeta}^{(\xi)} & \text{if } P_e\left(\mathbf{d}_{\zeta}^{(\xi)}\right) < P_e\left(\mathbf{pb}_{\zeta}^{(\xi-1)}\right) \\ \mathbf{pb}_{\zeta}^{(\xi-1)} & \text{if } P_e\left(\mathbf{d}_{\zeta}^{(\xi)}\right) \geq P_e\left(\mathbf{pb}_{\zeta}^{(\xi-1)}\right). \end{cases} \tag{63}$$

Then, the global best position of the ξth generation $\mathbf{gb}^{(\xi)} = \left[gb_1^{(\xi)}, \ldots, gb_{N_T}^{(\xi)}\right]^T$ is calculated based on

$$\mathbf{gb}^{(\xi)} = \begin{cases} \mathbf{pb}_{\zeta_{best}}^{(\xi)} & \text{if } P_e\left(\mathbf{pb}_{\zeta_{best}}^{(\xi)}\right) < P_e\left(\mathbf{gb}^{(\xi-1)}\right) \\ \mathbf{gb}^{(\xi-1)} & \text{if } P_e\left(\mathbf{pb}_{\zeta_{best}}^{(\xi)}\right) \geq P_e\left(\mathbf{gb}^{(\xi-1)}\right). \end{cases} \tag{64}$$

Furthermore, the velocity of the ζth particle during the ξth generation is also updated similarly to the dQPSO, according to

$$\begin{aligned} \mathrm{v}_{\zeta,n_T}^{(\xi)} = {} & g \cdot \mathrm{v}_{\zeta,n_T}^{(\xi-1)} + u_1 \cdot c_1 \cdot \Re\left\{pb_{\zeta,n_T}^{(\xi)} - d_{\zeta,n_T}^{(\xi)}\right\} \\ & + j \cdot u_2 \cdot c_2 \cdot \Im\left\{pb_{\zeta,n_T}^{(\xi)} - d_{\zeta,n_T}^{(\xi)}\right\} \\ & + u_3 \cdot c_1 \cdot \Re\left\{gb_{n_T}^{(\xi)} - d_{\zeta,n_T}^{(\xi)}\right\} \\ & + j \cdot u_4 \cdot c_2 \cdot \Im\left\{gb_{n_T}^{(\xi)} - d_{\zeta,n_T}^{(\xi)}\right\}, \end{aligned} \tag{65}$$

if the ζth particle was observed by the DHA during the ξth generation, or

$$\begin{aligned} \mathrm{v}_{\zeta,n_T}^{(\xi)} = {} & g \cdot \mathrm{v}_{\zeta,n_T}^{(\xi-1)} + u_3 \cdot c_2 \cdot \Re\left\{gb_{n_T}^{(\xi)} - d_{\zeta,n_T}^{(\xi)}\right\} \\ & + j \cdot u_4 \cdot c_2 \cdot \Im\left\{gb_{n_T}^{(\xi)} - d_{\zeta,n_T}^{(\xi)}\right\}. \end{aligned} \tag{66}$$

if it was not, with the difference that the parameters c_1, c_2 are now generation-based [55], as encapsulated in

$$c_1 = -2(\xi/\Xi) + 2.5 \tag{67}$$

$$c_2 = 2(\xi/\Xi) + 0.5. \tag{68}$$

With the aid of the sigmoid function of (56) in the dQPSO, each particle's velocity was confined to the $[0, M-1]$ range. In the cQPSO the velocity range for each particle's dimension is

$$V = [-V_{\max}, V_{\max}] + j \cdot [-V_{\max}, V_{\max}], \tag{69}$$

where we have opted for $V_{\max} = 1.2$, and the updated velocity of the ζth particle's n_Tth dimension during the ξth generation is guaranteed to be in that range by applying

$$\Re\left\{\mathrm{v}_{\zeta,n_T}^{(\xi)}\right\} = \begin{cases} -V_{\max}, & \Re\left\{\mathrm{v}_{\zeta,n_T}^{(\xi)}\right\} < -V_{\max} \\ \Re\left\{\mathrm{v}_{\zeta,n_T}^{(\xi)}\right\}, & -V_{\max} \leq \Re\left\{\mathrm{v}_{\zeta,n_T}^{(\xi)}\right\} \leq V_{\max} \\ V_{\max}, & \Re\left\{\mathrm{v}_{\zeta,n_T}^{(\xi)}\right\} > V_{\max} \end{cases}$$

$$\Im\left\{\mathrm{v}_{\zeta,n_T}^{(\xi)}\right\} = \begin{cases} -V_{\max}, & \Im\left\{\mathrm{v}_{\zeta,n_T}^{(\xi)}\right\} < -V_{\max} \\ \Im\left\{\mathrm{v}_{\zeta,n_T}^{(\xi)}\right\}, & -V_{\max} \leq \Im\left\{\mathrm{v}_{\zeta,n_T}^{(\xi)}\right\} \leq V_{\max} \\ V_{\max}, & \Im\left\{\mathrm{v}_{\zeta,n_T}^{(\xi)}\right\} > V_{\max} \end{cases}$$

Furthermore, if an updated velocity is equal to zero, then it is randomly selected as in

$$\mathrm{v}_{\zeta,n_T}^{(\xi)} = 2 \cdot (u - 0.5) \cdot \gamma \cdot (V_{\max} + j \cdot V_{\max}), \tag{70}$$

where $u \in \mathcal{U}(0, 1)$ is randomly selected based on the uniform distribution and $\gamma = 0.1$ [30].

Another difference between the dQPSO and the cQPSO is the update of a particle's position, which is updated with the aid of a different methodology in the cQPSO, based on whether the particle was obtained during the operation of the DHA or not. More specifically, if a particle was not obtained during the DHA, then its position during the next generation is randomly selected in the search space S^{N_T}. Otherwise, its position is updated as in

$$\mathbf{d}_{\zeta}^{(\xi)} = \mathbf{d}_{\zeta}^{(\xi)} + \mathbf{v}_{\zeta}^{(\xi)}. \tag{71}$$

Again, the position is limited to the search space S^{N_T} of (62), when applying (58) of the dQPSO by replacing $(M-1)/2$ with $S_{\max}$.

4) DHA INITIALIZATION

During the first generation, the reference value δ in the DHA is initialized with the CF value of the output of the dQPSO $P_e(\mathbf{d}_{opt,discrete})$, since it is the best found transmission vector up to that point. During the $\xi > 1$ generation, δ is initialized with the CF value of the best particle of the previous generation, regardless of whether it was the global best particle or not. The reason that we opted for a different methodology in the cQPSO, with respect to that of the dQPSO described in Section IV-B4 is due to the infinite search space that the cQPSO deals with. It was more likely to find an improved

transmission vector $\mathbf{d}$ by starting from the best particle in hand, than from a randomly selected one in the cQPSO.

5) TERMINATION

Similarly to the dQPSO, the cQPSO is terminated after Ξ_c generations, when we have $\mathbf{d}_{opt,cont.} = \mathbf{gb}^{(\Xi_c)}$.

The complexity of the classical PSO, quantified in terms of the number of CFES, is equal to

$$C_{PSO} = Z \cdot \Xi, \tag{72}$$

while that of the QPSO is equal to

$$C_{QPSO} = A \cdot \Xi. \tag{73}$$

TABLE 2. Parameters of the 8-user MC-IDMA downlink.

Number of Users	$U = 8$
Number of AEs per User	$N_R = 1$
Number of AEs at the BS	$N_T = 4$
Modulation	QPSK $M = 4$
Channel Code	Turbo Convolutional Code, $R = 1/2$, 8 Trellis states, $I = 4$ iterations
Number of Subcarriers	$Q = 1024$
Cyclic Prefix	CP = 128
Normalized User Load	$U_L = U \cdot N_R/N_T = 2$
Interleaver Length	2048 bits per User
Channel Model	Extended Vehicular A (EVA) [56]
Mobile Velocity	$v = 30$ km/h
Sampling Frequency	$f_s = 15.36$ MHz
Carrier Frequency	$f_c = 2.5$ GHz
Normalized Doppler Frequency	$f_d = 4.52 \cdot 10^{-6}$
Channel Estimation	Perfect

V. SIMULATION RESULTS

In order to characterize the performance of the proposed dQPSO and cQPSO algorithms in our MUT application, let us consider a rank-deficient system supporting $U = 8$ single-antenna users, while the BS is equipped with $N_T = 4$ transmit antennas, resulting in a normalized user load of $U_L = 2$. The modulation scheme is QPSK, while the channel code employed is a turbo convolutional code having a rate of $R = 1/2$, 8 trellis states and $I = 4$ inner decoding iterations. The number of subcarriers is equal to $Q = 1024$ and the interleaver length is 2048 bits per user. The system parameters are gathered in Table 2.

Figure 9 compares the BER performance of the dQPSO to that of the dPSO, when only a discrete-valued search is allowed for finding the optimal transmission vector in the downlink of the MC-IDMA system. Various combinations of the population size Z_d, the number of generations Ξ_d and the number of CFEs per generation for the dQPSO Ξ_d were

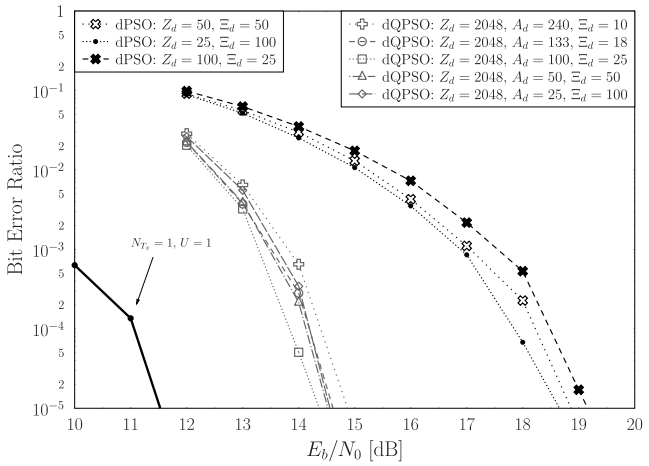

FIGURE 9. BER performance with respect to E_b/N_0 of the downlink system of Fig. 2, when only a discrete-valued PSO or QPSO search is used for finding the transmitted vector, for various combinations of population size Z_d, number of generations Ξ_d and number of CFEs per generation in the case of dQPSO A_d. The system parameters are summarized in Table 2.

evaluated, with all of them exhibiting similar complexity of at most 2500 CFEs. For the dQPSO a population size of $Z_d = 2048$ particles was selected, hence requiring $n = \log_2(Z_d) = 11$ qubits, due to the limited computation resources that a classical computer offers, when simulating the behaviour of a quantum computer. In theory, the population size may be quadrupled without increasing the algorithm's computational complexity expressed in terms of the number of CFEs, by adding two more qubits. At a BER of 10^{-5}, the average power gain of the dQPSO with respect to the dPSO is 4.4 dB.

The dPSO characterized in Fig. 9 performs better, when more generations are allowed, while the dQPSO achieved its best performance, when the number of generations Ξ_d was lower than the number of CFEs allowed per generation A_d. Based on our simulations, this also depends on the size of the database, or, equivalently, on the population size, since the DHA may require more CFEs for finding sufficiently good particles. It should be noted that in a database of $Z_d = 2048$ entries the DHA described in [39] requires $A_d = 316$ CFEs on average. However, based on the Early-Stopping-aided DHA of [8], which may reduce the complexity of the DHA, it may be found that using $A_d = 240$ achieves a 90% success probability of finding the optimal particle in each generation. Based on Fig. 9, choosing $A_d = 100$ CFEs per generation results in the best BER performance, while succeeding in finding the optimal particle with as low as 27% success probability, when randomly initialized. On the other hand, when the DHA is deterministically initialized, as it occurs in the $\xi > 1$ generations of the dQPSO, the success probability of finding the optimal particle of the generation increases for a fixed number of CFEs per search [8], with the gain depending on the CF value of the particle initializing the DHA. All investigated rank-deficient scenarios are at least 2.5 dB away from the single-user single-stream scenario

at BER $= 10^{-5}$. Let us proceed in our discussions by using the specific combinations that offered the average performance of the dPSO and the dQPSO in Fig. 9, which are the $[Z_d = 50, \Xi_d = 50]$ and $[Z_d = 2048, A_d = 133, \Xi_d = 18]$ configurations, respectively.

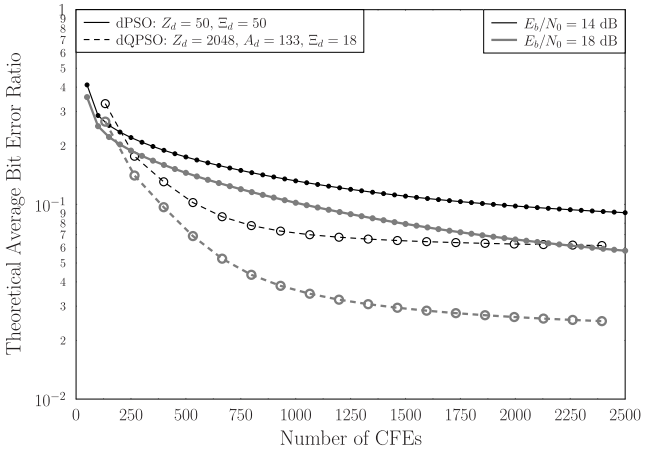

FIGURE 10. Error probability of (28) as a function of the number of CFEs in dPSO and dQPSO for $E_b/N_0 = 14$ dB and $E_b/N_0 = 18$ dB.

The high power gain of 4.4 dB on average, which was demonstrated in Fig. 9, in the scenario, where only a discrete-valued search is used for finding the perturbation vector may be further explained by investigating the global best CF value of (28) as a function of the computational complexity required, as illustrated in Fig. 10 for the E_b/N_0 values of 14 and 18 dB, where the dQPSO and the dPSO achieve a BER of $3 \cdot 10^{-4}$, respectively. The results were averaged over 100 independent simulations of the systems. Based on Fig. 10, we observe that the dQPSO initially requires a higher complexity for the first generation, whilst achieving a better CF value than the dPSO at its own first generation, but a worse CF value, when compared to that of the dPSO after three generations, which requires similar complexity. Since we have $A_d = 133$ CFEs per generation in the QPSO, after the first generation the complexity of the dQPSO is 133 CFEs. At the same time, the complexity of the classical dPSO after the first generation is equal to $Z_d = 50$ CFEs. After two generations, the complexity of the dPSO is $2 \cdot Z_d = 100$ CFEs, which is still lower than the complexity of the dQPSO after a single generation. However, an individual with lower average theoretical BER is found during the first generation of the dQPSO, than during the first generation of the dPSO. On the other hand, a better individual is found during the second generation of the dPSO than the one found during the first generation of the dQPSO. The fact that the dQPSO finds a better individual during its second generation ($2 \cdot A_d = 266$ CFEs) than the best individual found by the dPSO after its sixth generation (300 CFEs) for both E_b/N_0 values proves that even though the number of CFEs per generation is higher in the dQPSO, a better perturbation vector is found after having invested a lower number of CFEs. In other words, the benefit of the dQPSO manifests itself in terms of a steeper gradient of finding particles with lower CF values during the subsequent generations, as shown in Fig. 10, which manages to find a solution associated with the error probability of (28) equal to 0.09 by requiring 1835 fewer CFEs than the dPSO, when $E_b/N_0 = 14$ dB, or, alternatively, only at 26.6% of the complexity required by the dPSO. Moreover, the dQPSO not only arrives at a lower error probability floor, when compared to that of the dSPO, but also requires a lower complexity. For example, when $E_b/N_0 = 18$ dB, the dQPSO achieves half the error probability of the dPSO, while imposing 63% of the dPSO's complexity. The reason that the average BER depicted in Fig. 10 for $E_b/N_0 = 14$ and $E_b/N_0 = 18$ dB is not the same as that in Fig. 9 for the same power levels, is that the CF of (28), which is plotted in Fig. 10, assumes no channel coding, while the BER performance of Fig. 9 relies on channel coding. However, the MBER metric of (28) is sufficient for selecting the optimal transmission vector and the turbo convolutional code further reduces the system's BER. This is evident by comparing the dPSO's curve for $E_b/N_0 = 18$ dB and that of the dQPSO for $E_b/N_0 = 14$ dB in Fig. 10, which achieve a similar BER of $\sim$0.06 after 2500 CFEs, to their corresponding BER performances, when channel coding is invoked in Fig. 9 (white "x" at $E_b/N_0 = 18$ dB and white circle at $E_b/N_0 = 14$ dB), which are again similar and approximately BER $= 2.5 \cdot 10^{-4}$.

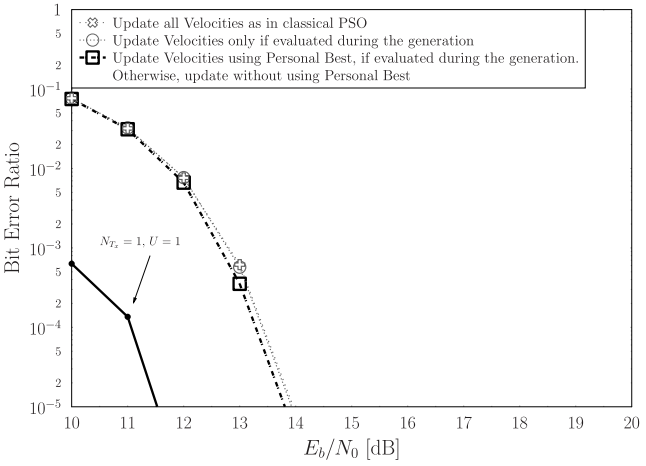

FIGURE 11. BER performance with respect to E_b/N_0 of the downlink system of Fig. 2, when only a discrete-valued QPSO search is used for finding the transmitted vector for $[Z_d, \Xi_d, A_d] = [2048, 18, 133]$. Three methodologies for updating the particles' velocities are evaluated. The system parameters are summarized in Table 2.

In Fig. 11 we compare three different methodologies for updating the velocities of a population's particles during the dQPSO. Even though their BER performance difference is low, we may observe that following the same methodology as in the classical dPSO yields similar results to the case, where only the velocities of the evaluated particles were updated during each generation. This occurs due to the fact that the position update of (57) has a random factor that changes the position of a particle even if its velocity remains the same throughout the generations. By using our proposed

methodology of (49) and (51), where the velocity of a particle is always updated based on the global best particle and also on the personal best particle only if that particle was evaluated during that generation, the performance improved by 0.15 dB. This may be explained by describing the proposed methodology as a combination of the previous two velocity updates. If the particle was evaluated during the present generation, its velocity should be updated as in the classical dPSO. Otherwise, its personal best position may be considered ''untrustworthy'', since it was not observed by the DHA, hence that particle should be guided to a ''better'' territory, by updating its velocity only based on the global best position. However, the performance gain achieved is minimal, when compared to the 2.3 dB loss with respect to the single-user single-stream full-rank scenario, where no precoding is required, since the system supports a single user.

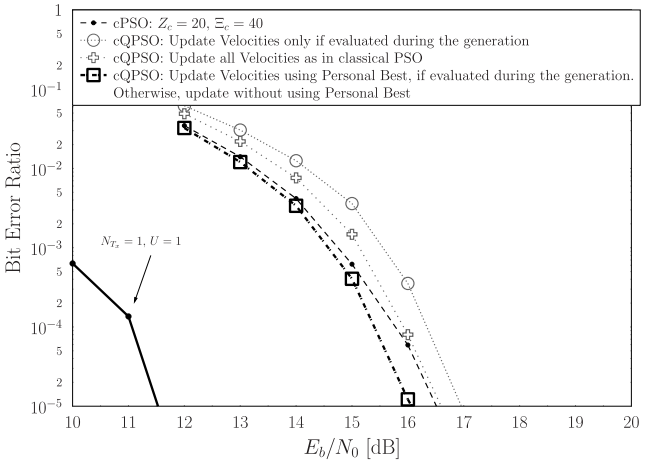

FIGURE 12. BER performance with respect to E_b/N_0 of the downlink system of Fig. 2, when a continuous-valued QPSO search associated with $[Z_c, \Xi_c, A_c] = [2048, 40, 20]$ is used after employing a discrete-valued classical PSO search for finding the transmitted vector. Three methodologies for updating the particles' velocities are evaluated. The system parameters are summarized in Table 2.

Similarly, in Fig. 12 we have evaluated the different methodologies for velocity updates in the case of cQPSO, following a classical dPSO search. Since in the continuous-valued search the position update does not include an independent random factor according to (71), if the velocity of a particle is not updated, then its position will continue to be beneficially updated towards the same direction, which may be towards even higher CF values. This is encapsulated in Fig. 12, where the aforementioned methodology (circle) performs worse than that of the classical cPSO (cross). Moreover, the cQPSO using the classical PSO's update methodology for the velocities is limited to the performance of the classical cPSO, since the inclusion of the personal best positions in the calculation of the velocities of particles that were not observed by the DHA may lead them to regions associated with high CF values. Based on this, our methodology proposed for the velocity updates of (49) and (51) in cQPSO, which is the same as in the dQPSO case, seems to offer a 0.5 dB gain, when compared to the classical cPSO's performance. This is attained by exploiting the personal best position of a particle only when it is worth it.

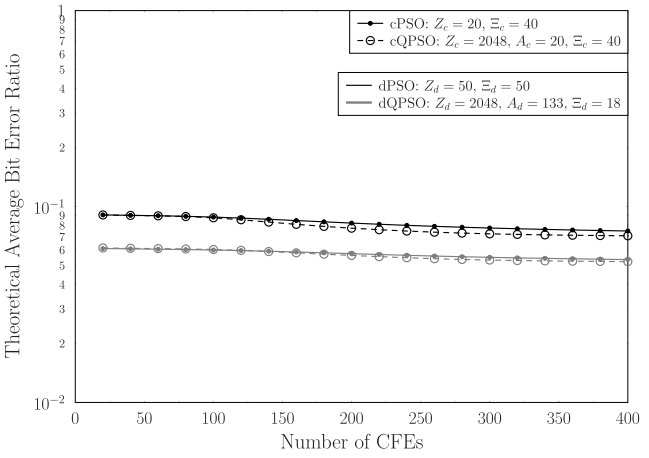

FIGURE 13. Error probability of (28) as a function of the number of CFEs in cPSO and cQPSO for $E_b/N_0 = 14$ dB following the operation of the dPSO or the dQPSO.

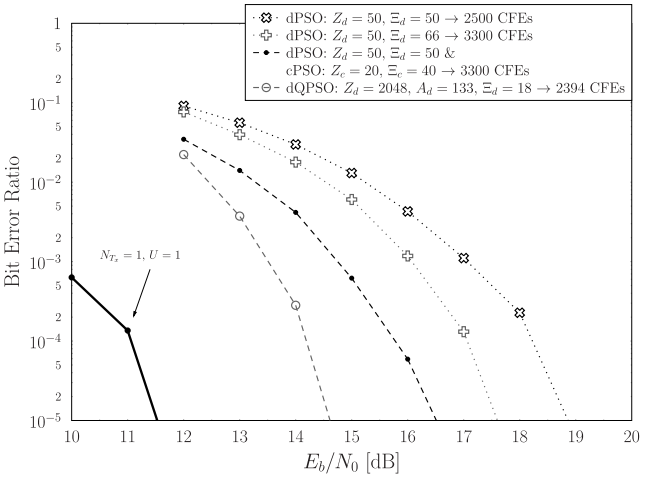

FIGURE 14. BER performance with respect to E_b/N_0 of the downlink system of Fig. 2, for evaluating the effect that a continuous-valued PSO search has to it. The system parameters are summarized in Table 2.

Figure 13 depicts the error probability of (28), when both discrete-valued and continuous-valued PSOs are used. We may conclude that the gain achieved by using the dQPSO instead of the dPSO is higher than that achieved by using the cQPSO instead of the cPSO. Nevertheless, the effect of the cQPSO is more evident, when the discrete-valued search is performed by the classical dPSO. The 0.02 uncoded BER gain obtained as a result of using a continuous-valued PSO after the dPSO at $E_b/N_0 = 14$ dB is expected to be further magnified, when channel coding is invoked. In other words, even though the effect of using a continuous-valued PSO seems to be minimal, when observing the uncoded error probability performance, it is actually more substantial, when investigating the system's overall performance, as exemplified in Fig. 14. In that figure, a fully classical

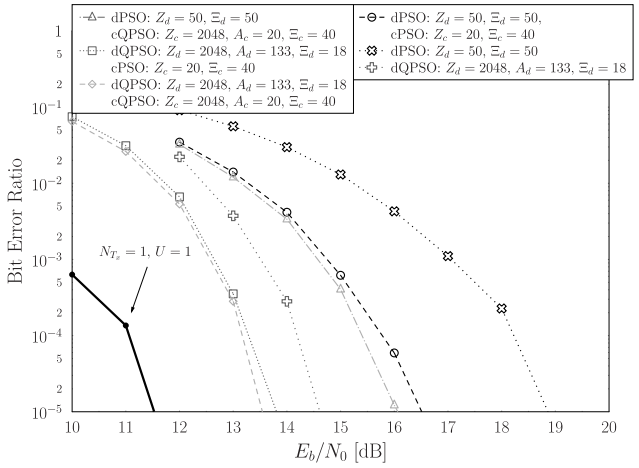

FIGURE 15. BER performance with respect to E_b/N_0 of the downlink system of Fig. 2, all the different discrete-valued and continuous-valued, classical and quantum search combinations. The system parameters are summarized in Table 2.

system employing both a dPSO associated with $[Z_d,\ \Xi_d] = [50, 66]$ and a cPSO associated with $[Z_c,\ \Xi_c] = [20, 40]$ is compared to a classical system, where only the dPSO is used in conjunction with $[Z_d,\ \Xi_d] = [50, 66]$. Both systems have the same complexity, but even though the $[Z_d,\ \Xi_d] = [50, 66]$ dPSO system performs 1.3 dB better than the lower-complexity $[Z_d,\ \Xi_d] = [50, 50]$ dPSO system at BER $= 10^{-5}$, it experiences a performance degraded by 1.07 dB at the same BER level, when compared to the aforementioned dPSO/cPSO system. We may conclude that by investing a higher complexity in the discrete-valued search is indeed capable of improving the system's BER performance, but eventually the discrete-valued search converges to a transmitted vector $\mathbf{d}$ that yields a higher BER than that of the vector $\mathbf{d}$ that would have been found by investing the same complexity as a continuous-valued search following the initial discrete-valued one. However, according to Fig. 14, by just using a dQPSO associated with $[Z_d, A_d, \Xi_d] = [2048, 133, 18]$ we may achieve a performance improved by 1.9 dB, when compared to the dPSO/cPSO system, while at the same time requiring fewer CFEs than the least complex dPSO associated with $[Z_d,\ \Xi_d] = [50, 50]$.

The BER performances of all investigated scenarios, namely of the dPSO, dQPSO, dPSO/cPSO, dPSO/cQPSO, dQPSO/cPSO and dQPSO/cQPSO systems, are illustrated in Fig. 15. Again, the dQPSO system outperforms all the three scenarios, which use the classical discrete-valued PSO. The employment of the continuous-valued QPSO results in a 0.5 dB gain with respect to the continuous-valued PSO at BER $= 10^{-5}$, when the dPSO is selected for the initial discrete-valued search, while that gain becomes 0.25 dB, when the dQPSO is used for the discrete-valued search. At the same time, there is an approximately 1 dB gain achieved by using the cQPSO at BER $= 10^{-5}$, when dQPSO is employed for the discrete-valued search, but 800 additional CFEs are required. Since all scenarios represent a rank-deficient system having a normalized user load of $U_L = 2$, they experience a performance loss with respect to the single-user and single-stream scenario, with the dQPSO/cQPSO system yielding the lowest power loss of 2 dB. The complexities of the systems, as well as their performance degradation compared to the single-user, single-stream scenario are gathered in Table 3. We may conclude that the improvement that the dQPSO achieves, when compared to its classical counterpart dPSO, is much higher than that of the cQPSO, when compared to the cPSO. Furthermore, based on Fig. 10, Fig. 13 and Fig. 15 it is evident that the discrete-valued search dominates the overall system's performance, since it finds the "main" transmitted vector $\mathbf{d}$, the neighbourhood of which is searched by the continuous-valued PSO.

TABLE 3. Complexity and performance loss.

Search Algorithms	Complexity (CFEs)	Power Loss (dB)
dQPSO	2394	3.08
dPSO	2500	7.33
dQPSO / cQPSO	3194	2.01
dQPSO / cPSO	3194	2.27
dPSO / cQPSO	3300	4.53
dPSO / cPSO	3300	4.98

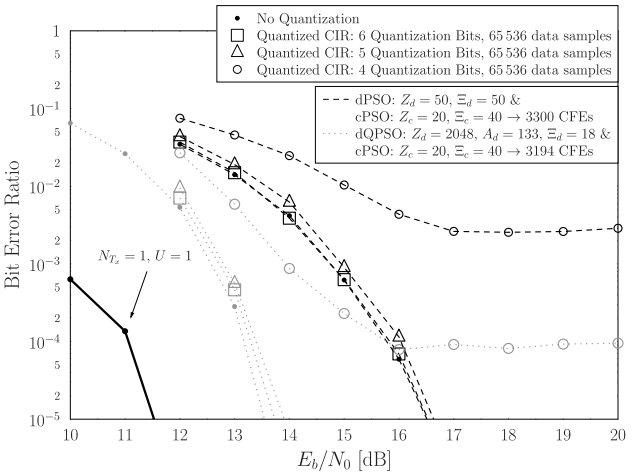

FIGURE 16. BER performance with respect to E_b/N_0 of the downlink system of Fig. 2, when channel quantization takes place at the mobile users, who transmit the quantized channel states to the BS through noiseless feedback channels. The system parameters are summarized in Table 2.

In Fig. 16 we investigate the sensitivity of the dPSO and dQPSO to channel quantization. So far, we have been assuming that the BS has perfect channel estimates of all channels. When FDD is adopted, the mobile users transmit quantized versions of their CSI to the BS via feedback channels. Let us assume that the feedback channels are noiseless, in order to focus our attention on the effect that the quantization precision has on the system's BER performance. We have

opted for using a codebook for quantizing the amplitude of each time-domain channel state between a single transmit antenna and a user, as well as a different codebook for quantizing the phases of the aforementioned channels [48], [57]. The k-means clustering algorithm [58], [59] was invoked for creating the two codebooks, using q number of quantization bits each, resulting in 2^q entries for each codebook. As we may observe in Fig. 16, when $q = 6$ or even $q = 5$ quantization bits are used for creating each of the codebooks, the associated performance of the resultant system is near-optimal, approaching the corresponding perfect CSI scenarios. On the other hand, when $q = 4$ quantization bits are used for creating each of the codebooks, the resultant performance is gravely degraded and tends to a BER floor. The proposed dQPSO experiences a lower sensitivity to the errors introduced by the channel quantization, since it achieves a BER floor 1.5 orders of magnitude lower than that yielded by the dPSO. It should be noted that the quantization errors result in an erroneous error probability expectation of (28) during the vector perturbation procedure, since the actual channels will be different. Nevertheless, the resilience to quantization errors may be viewed as a result of the densely populated search space that the dQPSO employs, making it possible to approach the – erroneously assumed – optimal transmit vector, given the quantized versions of the CSI, while being close to the true optimal transmit vector, when the actual CSI is similar to its quantized version.

VI. CONCLUSIONS

In this contribution we proposed two quantum-assisted bio-inspired algorithms for performing discrete-valued and continuous-valued heuristic search, namely the dQPSO as well as the cQPSO, and employed them for the vector perturbation procedure in the downlink of rank-deficient NOMA systems, while employing the MBER criterion for evaluating the legitimate candidates. Similarly to the classical PSO, the quality of the dQPSO depends on the allocation of its available complexity to the number of CFEs per generation and the number of generations, while the dQPSO substantially outperforms its classical equivalent according to Fig. 9 for a similar complexity. In Fig. 11 and Fig. 12 we considered the proposed methodology for updating a particle's velocity in the dQPSO and cQPSO, respectively. Moreover, Fig. 10 and Fig. 13 depicted the reasons why the contribution of the discrete-valued search is higher than that of the continuous-valued search, while demonstrating the superiority of the proposed dQPSO over the dPSO and the fact that the proposed cQPSO achieves a modest performance improvement, when compared to its classical counterpart.

The benefit of allocating a portion of the available complexity for performing a continuous-valued search after the discrete-valued search became evident in Fig. 14. Additionally, relying on Fig. 15 we may conclude that the dQPSO has the highest effect on the NOMA system's BER, followed by the presence or absence of a continuous-valued search for the effective transmit vector. The same conclusions are drawn based on Table 3, which summarizes the performance versus complexity of the system in Fig. 15. Finally, we found in Fig. 16 that the proposed dQPSO-aided search is less sensitive to quantization errors than the dPSO search, making the former even more suitable for realistic systems, when a quantum computer becomes available.

It should be noted that the proposed quantum-assisted algorithms may be tailored for use in other optimization problems in the field of wireless communications including, but not limited to, signal detection, channel estimation, or resource allocation, for achieving near-optimal performance, subject to the selected criterion, at a low computational complexity.

ACKNOWLEDGMENT

The use of the IRIDIS High Performance Computing Facility at the University of Southampton is acknowledged.

REFERENCES

[1] L. Hanzo, M. Münster, B. Choi, and T. Keller, *OFDM and MC-CDMA for Broadband Multi-User Communications, WLANs and Broadcasting*. New York, NY, USA: Wiley, 2003.

[2] L. L. Hanzo, Y. Akhtman, M. Jiang, and L. Wang, *MIMO-OFDM for LTE, WiFi and WiMAX: Coherent Versus Non-coherent and Cooperative Turbo Transceivers*. New York, NY, USA: Wiley, 2010.

[3] Y. Saito, Y. Kishiyama, A. Benjebbour, T. Nakamura, A. Li, and K. Higuchi, "Non-orthogonal multiple access (NOMA) for cellular future radio access," in *Proc. IEEE Veh. Technol. Conf. (VTC Spring)*, Jun. 2013, pp. 1–5.

[4] L. Dai, B. Wang, Y. Yuan, S. Han, C. L. I, and Z. Wang, "Non-orthogonal multiple access for 5G: Solutions, challenges, opportunities, and future research trends," *IEEE Commun. Mag.*, vol. 53, no. 9, pp. 74–81, Sep. 2015.

[5] Z. Yang, Z. Ding, P. Fan, and G. K. Karagiannidis, "On the performance of non-orthogonal multiple access systems with partial channel information," *IEEE Trans. Commun.*, vol. 64, no. 2, pp. 654–667, Feb. 2016.

[6] M. Jiang and L. Hanzo, "Multiuser MIMO-OFDM for next-generation wireless systems," *Proc. IEEE*, vol. 95, no. 7, pp. 1430–1469, Jul. 2007.

[7] P. Botsinis, D. Alanis, S. X. Ng, and L. Hanzo, "Low-complexity soft-output quantum-assisted multiuser detection for direct-sequence spreading and slow subcarrier-hopping aided SDMA-OFDM systems," *IEEE Access*, vol. 2, pp. 451–472, May 2014.

[8] P. Botsinis, S. X. Ng, and L. Hanzo, "Fixed-complexity quantum-assisted multi-user detection for CDMA and SDMA," *IEEE Trans. Commun.*, vol. 62, no. 3, pp. 990–1000, Mar. 2014.

[9] L. Ping, L. Liu, K. Wu, and W. K. Leung, "Interleave division multiple-access," *IEEE Trans. Wireless Commun.*, vol. 5, no. 4, pp. 938–947, Apr. 2006.

[10] R. Zhang and L. Hanzo, "Three design aspects of multicarrier interleave division multiple access," *IEEE Trans. Veh. Technol.*, vol. 57, no. 6, pp. 3607–3617, Nov. 2008.

[11] P. Botsinis, D. Alanis, Z. Babar, S. X. Ng, and L. Hanzo, "Iterative quantum-assisted multi-user detection for multi-carrier interleave division multiple access systems," *IEEE Trans. Commun.*, vol. 63, no. 10, pp. 3713–3727, Oct. 2015.

[12] L.-L. Yang, "Multiuser transmission via multiuser detection: Altruistic-optimization and egocentric-optimization," in *Proc. IEEE 65th Veh. Technol. Conf. (VTC)*, Apr. 2007, pp. 1921–1925.

[13] H. Sung, S.-R. Lee, and I. Lee, "Generalized channel inversion methods for multiuser MIMO systems," *IEEE Trans. Commun.*, vol. 57, no. 11, pp. 3489–3499, Nov. 2009.

[14] E. Alsusa and C. Masouros, "Adaptive code allocation for interference management on the downlink of DS-CDMA systems," *IEEE Trans. Wireless Commun.*, vol. 7, no. 7, pp. 2420–2424, Jul. 2008.

[15] C. Masouros and E. Alsusa, "Two-stage transmitter precoding based on data-driven code-hopping and partial zero forcing beamforming for MC-CDMA communications," *IEEE Trans. Wireless Commun.*, vol. 8, no. 7, pp. 3634–3645, Jul. 2009.

[16] C. Masouros and E. Alsusa, "Dynamic linear precoding for the exploitation of known interference in MIMO broadcast systems," *IEEE Trans. Wireless Commun.*, vol. 8, no. 3, pp. 1396–1404, Mar. 2009.
[17] C. Masouros, "Correlation rotation linear precoding for MIMO broadcast communications," *IEEE Trans. Signal Process.*, vol. 59, no. 1, pp. 252–262, Jan. 2011.
[18] S. M. Razavi, T. Ratnarajah, and C. Masouros, "Transmit-power efficient linear precoding utilizing known interference for the multiantenna downlink," *IEEE Trans. Veh. Technol.*, vol. 63, no. 9, pp. 4383–4394, Nov. 2014.
[19] D. Kwon, W. Y. Yeo, and D. K. Kim, "A new precoding scheme for constructive superposition of interfering signals in multiuser MIMO systems," *IEEE Commun. Lett.*, vol. 18, no. 11, pp. 2047–2050, Nov. 2014.
[20] S. M. Razavi and T. Ratnarajah, "Adaptively regularized phase alignment precoding for multiuser multiantenna downlink," *IEEE Trans. Veh. Technol.*, vol. 64, no. 10, pp. 4863–4869, Oct. 2015.
[21] W. Yao, S. Chen, S. Tan, and L. Hanzo, "Minimum bit error rate multiuser transmission designs using particle swarm optimisation," *IEEE Trans. Wireless Commun.*, vol. 8, no. 10, pp. 5012–5017, Oct. 2009.
[22] C. B. Peel, B. M. Hochwald, and A. L. Swindlehurst, "A vector-perturbation technique for near-capacity multiantenna multiuser communication—Part I: Channel inversion and regularization," *IEEE Trans. Commun.*, vol. 53, no. 1, pp. 195–202, Jan. 2005.
[23] B. M. Hochwald, C. B. Peel, and A. L. Swindlehurst, "A vector-perturbation technique for near-capacity multiantenna multiuser communication—Part II: Perturbation," *IEEE Trans. Commun.*, vol. 53, no. 3, pp. 537–544, Mar. 2005.
[24] C.-B. Chae, S. Shim, and R. W. Heath, "Block diagonalized vector perturbation for multiuser MIMO systems," *IEEE Trans. Wireless Commun.*, vol. 7, no. 11, pp. 4051–4057, Nov. 2008.
[25] S.-H. Park, H.-S. Han, S. Lee, and I. Lee, "A decoupling approach for low-complexity vector perturbation in multiuser downlink systems," *IEEE Trans. Wireless Commun.*, vol. 10, no. 6, pp. 1697–1701, Jun. 2011.
[26] C. Masouros, M. Sellathurai, and T. Ratnarajah, "Computationally efficient vector perturbation precoding using thresholded optimization," *IEEE Trans. Commun.*, vol. 61, no. 5, pp. 1880–1890, May 2013.
[27] C. Masouros, M. Sellathurai, and T. Ratnarajah, "Vector perturbation based on symbol scaling for limited feedback MISO downlinks," *IEEE Trans. Signal Process.*, vol. 62, no. 3, pp. 562–571, Feb. 2014.
[28] S. P. Herath, D. H. N. Nguyen, and T. Le-Ngoc, "Vector perturbation precoding for multi-user CoMP downlink transmission," *IEEE Access*, vol. 3, pp. 1491–1502, 2015.
[29] W. Yao, S. Chen, and L. Hanzo, "Improved MMSE vector precoding based on the MBER criterion," in *Proc. IEEE Veh. Technol. Conf.*, Apr. 2009, pp. 1–5.
[30] W. Yao, S. Chen, and L. Hanzo, "Generalized MBER-based vector precoding design for multiuser transmission," *IEEE Trans. Veh. Technol.*, vol. 60, no. 2, pp. 739–745, Feb. 2011.
[31] L. Hanzo, H. Haas, S. Imre, D. O'Brien, M. Rupp, and L. Gyongyosi, "Wireless myths, realities, and futures: From 3G/4G to optical and quantum wireless," *Proc. IEEE*, vol. 100, pp. 1853–1888, May 2012.
[32] M. A. Nielsen and I. L. Chuang, *Quantum Computation and Quantum Information*. Cambridge, U.K.: Cambridge Univ. Press, 2000.
[33] S. Imre and F. Balázs, *Quantum Computing and Communications: An Engineering Approach*. New York, NY, USA: Wiley, 2005.
[34] S. Imre and L. Gyongyosi, *Advanced Quantum Communications: An Engineering Approach*. New York, NY, USA: Wiley, 2013.
[35] P. Botsinis, S. X. Ng, and L. Hanzo, "Quantum search algorithms, quantum wireless, and a low-complexity maximum likelihood iterative quantum multi-user detector design," *IEEE Access*, vol. 1, pp. 94–122, 2013.
[36] L. K. Grover, "A fast quantum mechanical algorithm for database search," in *Proc. 28th Annu. ACM Symp. Theory Comput.*, May 1996, pp. 212–219.
[37] L. K. Grover, "Quantum mechanics helps in searching for a needle in a haystack," *Phys. Rev. Lett.*, vol. 79, pp. 325–328, Jul. 1997.
[38] M. Boyer, G. Brassard, P. Høyer, and A. Tapp, "Tight bounds on quantum searching," *Fortschritte Phys.*, vol. 46, nos. 4–5, pp. 493–505, Jun. 1998.
[39] C. Durr and P. Høyer. (Jul. 1996). "A quantum algorithm for finding the minimum." [Online]. Available: https://arxiv.org/abs/quant-ph/9607014
[40] P. Botsinis, D. Alanis, Z. Babar, S. X. Ng, and L. Hanzo, "Noncoherent quantum multiple symbol differential detection for wireless systems," *IEEE Access*, vol. 3, pp. 569–598, May 2015.
[41] M. Y. Alias, S. Chen, and L. Hanzo, "Multiple-antenna-aided OFDM employing genetic-algorithm-assisted minimum bit error rate multiuser detection," *IEEE Trans. Veh. Technol.*, vol. 54, no. 5, pp. 1713–1721, Sep. 2005.
[42] S. Chen, A. Livingstone, and L. Hanzo, "Minimum bit-error rate design for space-time equalization-based multiuser detection," *IEEE Trans. Commun.*, vol. 54, no. 5, pp. 824–832, May 2006.
[43] S. Chen, L. Hanzo, and A. Livingstone, "MBER space-time decision feedback equalization assisted multiuser detection for multiple antenna aided SDMA systems," *IEEE Trans. Signal Process.*, vol. 54, no. 8, pp. 3090–3098, Aug. 2006.
[44] L. L. Hanzo and T. Keller, *OFDM and MC-CDMA: A Primer*. New York, NY, USA: Wiley, 2006.
[45] A. K. Dutta, K. V. S. Hari, and L. Hanzo, "Linear transceiver design for an amplify-and-forward relay based on the MBER criterion," *IEEE Trans. Commun.*, vol. 62, no. 11, pp. 3765–3777, Nov. 2014.
[46] D. J. Ryan, I. B. Collings, I. V. L. Clarkson, and R. W. Heath, "Performance of vector perturbation multiuser MIMO systems with limited feedback," *IEEE Trans. Commun.*, vol. 57, no. 9, pp. 2633–2644, Sep. 2009.
[47] P. Lu and H.-C. Yang, "Vector perturbation precoding for MIMO broadcast channel with quantized channel feedback," in *Proc. IEEE Global Telecommun. Conf.*, Nov./Dec. 2009, pp. 1–5.
[48] S. P. Herath, D. H. N. Nguyen, and T. Le-Ngoc, "Vector perturbation precoding under quantized CSI," *IEEE Trans. Veh. Technol.*, vol. 65, no. 1, pp. 420–427, Jan. 2016.
[49] E. Aïmeur, G. Brassard, and S. Gambs, "Quantum speed-up for unsupervised learning," *Mach. Learn.*, vol. 90, no. 2, pp. 261–287, Feb. 2013.
[50] D. Oliveira, P. B. M. de Sousa, and R. V. Ramos, "Quantum search algorithm using quantum bit string comparator," in *Proc. IEEE Int. Telecommun. Symp.*, Sep. 2006, pp. 582–585.
[51] G. Brassard, F. Dupuis, S. Gambs, and A. Tapp. (Jun. 2011). "An optimal quantum algorithm to approximate the mean and its application for approximating the median of a set of points over an arbitrary distance." [Online]. Available: http://arxiv.org/abs/1106.4267
[52] Z. Babar, P. Botsinis, D. Alanis, S. X. Ng, and L. Hanzo, "The road from classical to quantum codes: A hashing bound approaching design procedure," *IEEE Access*, vol. 3, pp. 146–176, 2015.
[53] Y. Shi and R. C. Eberhart, "Empirical study of particle swarm optimization," in *Proc. Congr. Evol. Comput.*, vol. 3. Jul. 1999, pp. 1945–1950.
[54] K. Veeramachaneni, L. Osadciw, and G. Kamath, "Probabilistically driven particle swarms for optimization of multi valued discrete problems: Design and analysis," in *Proc. IEEE Swarm Intell. Symp.*, Apr. 2007, pp. 141–149.
[55] A. Ratnaweera, S. K. Halgamuge, and H. C. Watson, "Self-organizing hierarchical particle swarm optimizer with time-varying acceleration coefficients," *IEEE Trans. Evol. Comput.*, vol. 8, no. 3, pp. 240–255, Jun. 2004.
[56] S. Sesia, I. Toufik, and M. Baker, Eds., *LTE—The UMTS Long Term Evolution: From Theory to Practice*. New York, NY, USA: Wiley, 2009.
[57] D. Yang, L.-L. Yang, and L. Hanzo, "Performance of SDMA systems using transmitter preprocessing based on noisy feedback of vector-quantized channel impulse responses," in *Proc. IEEE Veh. Technol. Conf.*, Apr. 2007, pp. 2119–2123.
[58] S. Lloyd, "Least squares quantization in PCM," *IEEE Trans. Inf. Theory*, vol. 28, no. 2, pp. 129–137, Mar. 1982.
[59] A. Gersho and R. M. Gray, *Vector Quantization and Signal Compression*. Norwell, MA, USA: Kluwer, 1991.

PANAGIOTIS BOTSINIS (S'12–M'15) received the M.Eng. degree from the School of Electrical and Computer Engineering, National Technical University of Athens, Greece, in 2010, and the M.Sc. degree (Hons.) and Ph.D. degrees in wireless communications from the University of Southampton, U.K., in 2011 and 2015, respectively. He is currently a Research Fellow with the Southampton Wireless Group, School of Electronics and Computer Science, University of Southampton, U.K. Since 2010, he has been a member of the Technical Chamber of Greece.

His research interests include quantum-assisted communications, quantum computation, iterative detection, OFDM, MIMO, multiple access systems, coded modulation, channel coding, cooperative communications, and combinatorial optimization.

DIMITRIOS ALANIS (S'13) received the M.Eng. degree in electrical and computer engineering from the Aristotle University of Thessaloniki in 2011, and the M.Sc. degree in wireless communications from the University of Southampton in 2012. He is currently pursuing the Ph.D. degree with the Southampton Wireless Group, School of Electronics and Computer Science, University of Southampton.

His research interests include quantum computation and quantum information theory, quantum search algorithms, cooperative communications, resource allocation for self-organizing networks, bio-inspired optimization algorithms, and classical and quantum game theory.

ZUNAIRA BABAR received the B.Eng. degree in electrical engineering from the National University of Science and Technology, Islamabad, Pakistan, in 2008, and the M.Sc. degree (Hons.) and Ph.D. degree in wireless communications from the University of Southampton, U.K., in 2011 and 2015, respectively. She is currently a Research Fellow with the Southampton Wireless Group, University of Southampton.

Her research interests include quantum error correction codes, channel coding, coded modulation, iterative detection, and cooperative communications.

HUNG VIET NGUYEN received the B.Eng. degree in electronics and telecommunications from the Hanoi University of Science and Technology, Hanoi, Vietnam, in 1999, the M.Eng. degree in telecommunications from the Asian Institute of Technology, Bangkok, Thailand, in 2002, and the Ph.D. degree in wireless communications from the University of Southampton, Southampton, U.K., in 2013. Since 1999, he has been a Lecturer with the Post and Telecommunications Institute of Technology, Vietnam. He is currently involved in the OPTIMIX and CONCERTO European projects. He is also a Post-Doctoral Researcher with the Southampton Wireless Group, University of Southampton, U.K.

His research interests include cooperative communications, channel coding, network coding, and quantum communications.

DARYUS CHANDRA (S'13) received the M.Eng. degree in electrical engineering from Universitas Gadjah Mada, Indonesia, in 2014. He is currently pursuing the Ph.D. degree with the Southampton Wireless Group, School of Electronics and Computer Science, University of Southampton. He is a recipient of scholarship award from Indonesia Endowment Fund for Education.

His research interests include channel codes, quantum error correction codes, and quantum communications.

SOON XIN NG (S'99–M'03–SM'08) received the B.Eng. degree (Hons.) in electronics engineering and the Ph.D. degree in wireless communications from the University of Southampton, Southampton, U.K., in 1999 and 2002, respectively. From 2003 to 2006, he was a Post-Doctoral Research Fellow, where he was involved in collaborative European research projects known as SCOUT, NEWCOM, and PHOENIX. Since 2006, he has been a member of academic staff with the School of Electronics and Computer Science, University of Southampton. He is currently involved in the OPTIMIX and CONCERTO European projects as well as the IUATC and UC4G projects. He is also an Associate Professor of Telecommunications with the University of Southampton. He has authored over 180 papers and co-authored two John Wiley/IEEE Press books in his research field.

His research interests include adaptive coded modulation, coded modulation, channel coding, space-time coding, joint source and channel coding, iterative detection, OFDM, MIMO, cooperative communications, distributed coding, quantum error correction codes, and joint wireless-and-optical-fiber communications. He is currently a Chartered Engineer and a fellow of the Higher Education Academy, U.K.

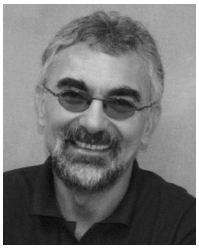

LAJOS HANZO (M'91–SM'92–F'04) received the degree in electronics and the Ph.D. degree in 1976 and 1983, respectively. In 2009, he was awarded the honorary doctorate Doctor Honoris Causa by the Technical University of Budapest. During his 38-year career in telecommunications, he has held various research and academic posts in Hungary, Germany, and the U.K. Since 1986, he has been with the School of Electronics and Computer Science, University of Southampton, U.K., where he holds the chair in telecommunications. He has successfully supervised about 100 Ph.D. students, co-authored 20 John Wiley/IEEE Press books on mobile radio communications totaling in excess of 10 000 pages, published over 1500 research entries at the IEEE Xplore, acted as a TPC and General Chair of the IEEE conferences, presented keynote lectures. He received a number of distinctions. He is currently directing a 100-strong Academic Research Team, where he is involved in a range of research projects in the field of wireless multimedia communications sponsored by industry, the Engineering and Physical Sciences Research Council, U.K., the European Research Council's Advanced Fellow Grant, and the Royal Society's Wolfson Research Merit Award. He is an Enthusiastic Supporter of industrial and academic liaison and he offers a range of industrial courses.

Dr. Lajos is a fellow of the Royal Academy of Engineering, the Institution of Engineering and Technology, and the European Association for Signal Processing. He is also a Governor of the IEEE Vehicular Technology Society. From 2008 to 2012, he was the Editor-in-Chief of the IEEE Press and a Chaired Professor with Tsinghua University, Beijing. He has authored over 22 000 citations.